METEOROLOGICAL APPLICATIONS
Meteorol. Appl. **18**: 334–353 (2011)
Published online in Wiley Online Library
(wileyonlinelibrary.com) DOI: 10.1002/met.284

RMetS
Royal Meteorological Society

Review
Global precipitation measurement

Chris Kidd[a]* and George Huffman[b,c]

[a] *Earth System Science Interdisciplinary Center, University of Maryland, College Park, MD, USA and NASA/Goddard Space Flight Center, Greenbelt, 20740 MD, USA*
[b] *Science Systems and Applications Inc., Lanham, 20706 MD, USA*
[c] *NASA/Goddard Space Flight Center, Greenbelt, 20771 MD, USA*

ABSTRACT: The quantification of precipitation on a global scale is critical for applications ranging from climate monitoring to water resource management. Conventional observations through surface gauge networks provide the most direct measure of precipitation, although these are very much limited to land areas, with very few *in situ* measurements over the oceans. Weather radars, although providing a spatial measure of precipitation, are limited in extent and number. Satellite observations offer an unrivalled vantage point to observe precipitation on a global basis. Since precipitation is spatially and temporally highly variable, satellites are able to provide temporal and spatial samples commensurate with many precipitation characteristics. This paper provides an overall review of global precipitation estimation, providing an outline of conventional measurements, the basis of the satellite systems used in the observation of precipitation, and the generation, availability and validation of the derived precipitation products. Finally, future satellite precipitation missions are presented. Copyright © 2011 Royal Meteorological Society

KEY WORDS precipitation; satellite observations; infrared; microwave

Received 13 May 2011; Revised 27 June 2011; Accepted 11 July 2011

1. Introduction

Precipitation is a fundamental component of the climate system and of the global water cycle. Within the water cycle, water vapour condenses into clouds from which precipitation may fall, returning water from the atmosphere to the surface, providing a primary source of fresh water vital to life on Earth. The monitoring and measurement of precipitation is crucial to our well-being; too much rainfall endangers life and property, while too little causes droughts that impact agriculture and can cause starvation. Precipitation also has an economic value, playing a key role in water resource management and agribusinesses (Kidd *et al*., 2009; Thornes *et al*., 2010). It is a driver in the evolution of the landscape around us, both through sustaining the natural vegetation, and also through erosional processes; it is also a factor in disposition of atmospheric pollution and in the transport of nutrients and pollution (Michaelides *et al*., 2009).

The mean annual global rainfall is calculated to be about 1000 mm; Michaelides *et al*. (2009) quote 1050 mm, while Legates and Willmott (1990) calculate a mean total of 1123 mm. However, the mean rainfall masks substantial regional and temporal differences. Some places receive on average no measurable rainfall each year, while others receive in excess of 10 000 mm each year. Local year-on-year variations can be a factor of two or more. The distribution of global precipitation is governed by large-scale controls such that regional precipitation is strongly correlated to the climatology. However, the variability of precipitation increases with finer temporal and spatial resolution. As a result, quantitative precipitation measurements are particularly challenging with conventional observing systems. Gauges close to one another can be expected to provide similar measurements, but this similarity quickly diminishes with increasing distance, particularly in regions dominated by convective rainfall.

Within the climate system it is acknowledged that the atmosphere is the most unstable of the five major components of that system (IPCC, 2007). The most variable component within the atmosphere is water, which as water vapour is the strongest greenhouse gas. Water in the atmosphere can manifest itself in gas, liquid and ice phases, each change of phase absorbing or releasing energy. Movement of water vapour within the atmosphere transports energy both laterally and vertically, redistributing energy across the globe through the evaporation of water and release of precipitation. The net atmospheric moisture transfer from ocean to land is estimated to be $40 \pm 1 \times 10^3$ km^3 year^{-1} (Dai and Trenberth, 2002; Trenberth *et al*., 2007) or 3.2 ± 0.1

* Correspondence to: C. Kidd, Earth System Science Interdisciplinary Center, University of Maryland, College Park, 20740 MD, USA and NASA/Goddard Space Flight Center, Greenbelt, 20771 MD, USA.
E-mail: chris.kidd@nasa.gov

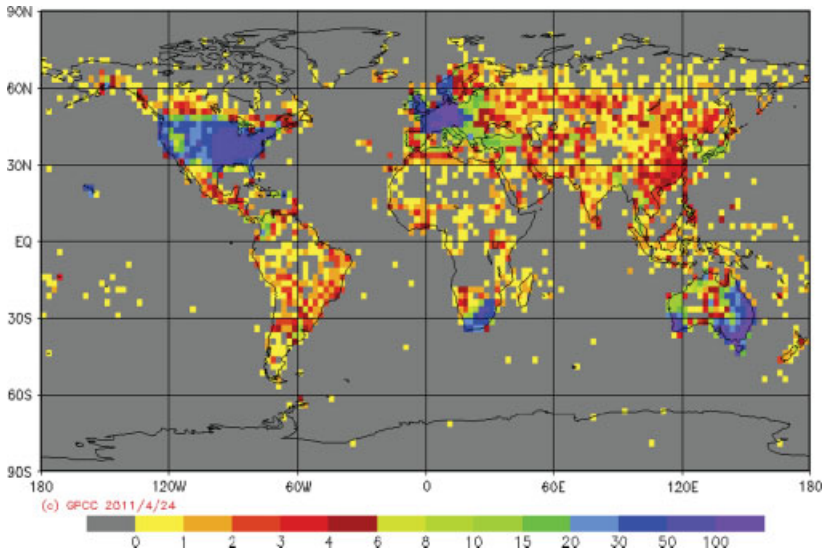

Figure 1. Number of gauges *per* 2.5° × 2.5° grid box used in the GPCC full data product (version 5) for June 2007.

PW of latent energy (equivalent to 80 W m^{-2} globally; Trenberth *et al*., 2009).

Changes in our climate will impact the distribution and amounts of precipitation across the globe. The most recent report of the Intergovernmental Panel on Climate Change (IPCC, 2007) notes that land-surface precipitation has shown a general increase of 5–10% *per* decade over the Northern Hemisphere middle to high latitudes. Over the tropical land regions increases of 2.4% $century^{-1}$ are quoted. These changes are reflected in the annual stream flow. However, changes in precipitation over the oceans are less clear, primarily due to lack of long-term oceanic measurements. Changes in precipitation are more pronounced for extreme precipitation events, both for intense precipitation events and occurrence of drought. New *et al*. (2001) note that precipitation over the global land surfaces (excluding Antarctica) has increased by 0.89 mm $decade^{-1}$ over the twentieth century, although they note that this change is small in comparison to the interannual and multi-decadal variability. Although most land areas have seen an increase in precipitation, notable exceptions include Tropical North Africa, southern Africa, Amazonia and western South America.

Gauges provide the most common and most direct measurement of point precipitation at the surface (New *et al*., 2001). These gauges can range from simple collecting vessels, such as 'standard' accumulation gauges to more complex tipping bucket gauges, weighing gauges, optical gauges and distrometers: all have their own characteristics with relative advantages and disadvantages. However, despite the fact that quantification of precipitation in all its forms over the globe is critical to a range of scientific and societal applications, the distribution of available gauges is quite varied. Much of the land masses (representing 25–30% of the Earth's surface) have measurement networks, although those networks with good gauge densities are limited, while measurements over the oceans are very sparse (see Figure 1). New *et al*. (2001) estimates the number of gauges worldwide to be about 250 000, while Strangeways (2007) puts the figure at 150 000. However, the number of gauges available globally varies with time and data requirements, with relatively few gauges available with hourly or sub-daily sampling. Furthermore, the lack of uniform data distribution results in only about 64 000 gauges being available for precipitation analyses.

Historically, quantitative precipitation measurements span a relatively short period in recent history. Although precipitation data are available in some regions/stations since the mid 1850s, early records vary in accessibility, completeness and consistency, leading to discontinuities and issues over quality control. Critically, the number of long term gauges is very much less, while the availability of data with shorter intervals (i.e daily or sub-daily) is even smaller (New *et al*., 1999; Jones *et al*., 2002). The physical characteristics of precipitation, particularly at finer spatial and temporal resolutions, necessitate frequent, systematic measurements. The current networks of surface observations are therefore often inadequate for the quantitative assessment of precipitation and its characteristics.

Despite the fact that gauges provide a physically direct measure of precipitation, they are prone to error. The main source of error is under-catch, primarily caused by wind effects around the gauge orifice (Peterson *et al*., 1998). In particular, the measurement of snow suffers from an under-catch of up to 50%. Legates and Willmott (1990) estimated the global under-catch to be about 11%, although this varies greatly from region to region. Differences in gauge type also affect the error characteristics and, although not common, changes in gauge type affect long-term records. Other insidious changes occur which are less easy to account for, such as observer errors and slow, long-term changes in the area surrounding the gauge.

On the global scale, the most useful products are the gridded data sets. These take the point source gauge data

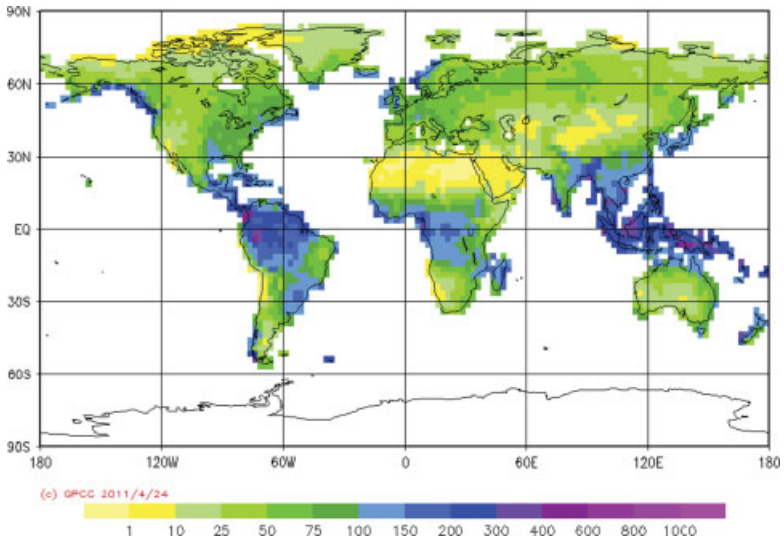

Figure 2. GPCC full data product of gauge-derived annual precipitation analysis at 2.5° × 2.5° resolution for 2007 (units in mm month^{-1}).

and map the information to a predefined temporal/spatial resolution grid. Notable surface gauge data sets include the Global Precipitation Climatology Centre (GPCC) gauge analyses that makes use of data from the Global Telecommunication System (GTS) network to generate monthly and daily global (land) products, augmented with other national network data when available, resulting in a database of approximately 64 000 gauges (Schneider *et al*., 2010). The Global Historical Climatology Network (GHCN) provides a dataset with 31 000 stations (New *et al*., 2001), although the number of gauges varies from year to year, with just 5500 in 1900. The main issue relates to how the gauge data are mapped onto the grid. One approach is to average the gauge records within each grid box; if no gauge information exists, the grid box is left empty (e.g. Hulme, 1994). Other schemes (e.g. Dai *et al*., 1997) use a distance-weighted scheme to fill grid boxes up to an empirically-derived distance. The GPCC global precipitation product (Rudolf *et al*., 1994; Schneider *et al*., 2010) uses a spherical mapping procedure to ensure continuous spatial and temporal land surface precipitation maps, an example of which is shown in Figure 2. The outcome of these different mapping techniques is that the end products inevitably differ, particularly in regions where the gauge density is low. Xie *et al*. (1996) found mean absolute differences between their extended precipitation gauge product and the GPCC product to be greater than 40% in regions with a single gauge *per* grid box. Furthermore, they note that interpolation tends to lead to an overestimation of heavy precipitation and an underestimation of low precipitation.

The use of weather radar addresses some of the issues of rain gauge coverage, at least where radar exists. In particular it provides a spatial measurement of precipitation rather than the point measurements provided by gauges. Standard weather radars generally operate at low frequencies, usually C-band (4–8 GHz) and S-band (2–4 GHz) but X-band (8–12 GHz) may also be used. The radar system emits a beam of microwave energy that is backscattered from particles in the atmosphere, which can then be converted into a measure of rainfall intensity. Unfortunately, the backscattered radiation is dependent upon the drop size distribution, which can vary considerably across the range of precipitation regimes (see Anagnostou *et al*., 1999a, 1999b; Krajewski *et al*., 2006). Problems also arise from range effects due to 'lifting' of the beam with range so that precipitation may be undetected (e.g. Kitchen and Jackson, 1993), while close to the radar false returns from ground objects may result. The introduction of dual-polarization on many new radar systems is designed to address these problems (Bringi *et al*., 2004). Unfortunately, weather radar networks tend to replicate the regional coverage of good gauge networks. Ultimately, the spatial coverage of gauge or radar networks is inadequate to monitor and quantify precipitation on a global basis.

In contrast, satellite observations of precipitation provide synoptic scale information that can be used to provide estimates on a global basis at scales that are commensurate with the needs of the user community, albeit with issues about accuracy. This paper therefore provides an overview of global precipitation measurements that can be derived from satellite observations. Section 2 provides a summary of the meteorological satellites and sensors used in the retrieval of precipitation. Section 3 examines the different methodologies and techniques to derive precipitation estimates from the satellite observations. The range of precipitation products currently available will be explored in Section 4, while the final section provides an overview of future satellite systems with precipitation capabilities.

2. Background

The first Television InfraRed Observing Satellite (TIROS-1) initiated meteorological observations of the Earth from space in April 1960 (Fritz and Wexler, 1960).

Table I. Summary of commonly-used satellite instrumentation for precipitation estimation.

Instrument	Satellite	Channels	Bands	Resolution (km)	Sampling
AVHRR	NOAA/MetOp	5	VIS-IR	1	Twice daily
SEVIRI	MSG	11	VIS-IR	1–3	15 min
GOES imager	GOES	5	VIS-IR	1–4	30 min
MODIS	Aqua/Terra	36	VIS-IR	0.25–1	Twice daily
SSM/I	DMSP	7	19–85 GHz	12.5–25	Twice daily
SSMIS	DMSP	11	19–183 GHz	13–45	Twice daily
TMI	TRMM	9	10–85 GHz	5–25	Twice 2-days
AMSU	NOAA/MetOp	5	23.8–183 GHz	20–50	Twice daily
MHS	NOAA/MetOp	5	89–190 GHz	17–50	Twice daily
AMSR	Aqua	12	6–85 GHz	5–25	Twice daily
PR	TRMM	1	13.6 GHz	5	Twice 3-days
CPR	CloudSat	1	94 GHz	1.4	Once 16-days

The World Meteorological Organisation (WMO) established the World Weather Watch programme in 1963 to co-ordinate the observational capability of surface and satellite observations, including the network of operational geostationary (GEO) and polar-orbiting meteorological satellites. The Global Observing System (GOS; WMO, 2005) was charged with providing long-term stable data sets required by international organizations and the user community. Meteorological satellites have been at the forefront of Earth observation with improvements in satellite and sensor technology to provide the current range of operational meteorological observations and quantitative information on precipitation from the satellite observations. Meteorological satellites can be divided in to two broad categories: GEO satellites and Low Earth Orbiting (LEO) satellites, which include polar-orbiting satellites. Table I summarizes the main instrumentation used for the estimation of precipitation, covering both visible (VIS) and infrared (IR) sensors and those in the microwave (MW) region of the spectrum.

2.1. GEO observation systems

GEO satellites orbit the Earth about 35 800 km above the Equator such that they orbit at the same rate as the Earth turns, appearing stationary relative to a location on the Earth's surface. Each GEO satellite is able to view about one third of the Earth's surface, but due to increasing scan angle towards the extremities of the imagery degrading the usability of the data, five operational GEO satellites are required to ensure full West–East (and $\sim$70 °N to 70 °S) coverage. From their position they are able to provide imagery on a frequent and regular basis. Current primary GEO satellites include the Meteosat Second Generation satellites (MSG; Schmetz *et al*., 2002) operated by the European Organisation for the Exploitation of Meteorological Satellites (EUMETSAT), two U.S. operated Geostationary Operational Environmental Satellite (GOES; Menzel and Purdom, 1994), the Feng-Yun-2 satellites from China (http://www.fas.org/spp/guide/china/earth/fy-2.htm#ref625), and the Japanese Multifunctional Transport Satellite (MTSAT) series (Yoshiro, 2002).

Although the sensor technologies vary among GEO systems, they share a number of common capabilities. They provide VIS and IR sensors with nominal resolutions of 1 km $\times$ 1 km and 4 km $\times$ 4 km, respectively, acquiring images every 30 min although some GEO satellites, such as MSG, provide images every 15 min. Newer sensors also provide rapid scanning capabilities that allow limited-area sub-minute sampling. Imagery from GEO sensors provide baseline observations across the Vis/IR region of the spectrum, although newer sensors provide greater detail. The SEVIRI sensor on the Meteosat Second Generation (MSG) satellite provides multispectral observations in 11 channels and allows greater potential for rainfall retrievals and microphysical analysis of cloud-top characteristics (such as cloud drop radii and phase) to be retrieved (Levizzani *et al*., 2001).

2.2. LEO observing systems

Observations from LEO orbiting satellites complement the observations from GEO-based instrumentation. LEO satellites can be subdivided into Sun-synchronous and non-Sun-synchronous missions. Operational meteorological satellites fall into the former category, with orbital characteristics such that they cross the Equator at the same local time on each orbit, providing up to two overpasses daily. Sensors typically include both multichannel VIS and IR sensors and passive microwave (PMW) sounders and imagers, the latter being capable of more direct measurements of precipitation. Current operational polar-orbiting satellites include the National Oceanic and Atmospheric Administration (NOAA) satellites (Goodrum *et al*., 2000) and EUMETSAT's MetOp series (Klaes *et al*., 2007). These satellites orbit the Earth once every 98 min at an altitude of about 850 km, carrying a wide range of instrumentation including the third-generation Advanced Very High Resolution Radiometer (AVHRR; Kidwell *et al*., 1991) and the Microwave Humidity Sounder (MHS).

One of the longest data sets of meteorological satellite observations has come from the operational AVHRR. This instrument provides observations at five wavelengths from the visible through to the thermal infrared

at a resolution of about 1 km. The sensor provides cross-track measurements with a swath width of about 3000 km, allowing the Earth to be covered twice-daily. More recently the Moderate-Resolution Imaging Sensor (MODIS), carried onboard the Terra and Aqua satellites, has gathered more detailed measurements across the VIS/IR in 36 spectral bands enabling greater spectral detail and greater spatial resolution down to 250 m.

The first PMW sensor, the Electrically Scanning Microwave Radiometer (ESMR), flew on Nimbus-5 and Nimbus-6 and paved the way for the Scanning Multichannel Microwave Radiometer (SMMR) on Nimbus-7. SMMR, launched in 1978, provided dual polarized observations across a range of frequencies from 6 to 37 GHz. In 1987 the first fully calibrated multichannel microwave radiometer, the Special Sensor Microwave/Imager (SSM/I) was launched on the Defense Meteorological Satellite Program (DMSP) series of satellites. These sensors provide observations from 18 to 85 GHz, the latter being particularly useful for rainfall estimation over land (Barrett *et al*., 1988). The SSM/I series of sensors have been the mainstay of information from microwave imagers since 1987, but the follow-on Special Sensor Microwave Imager-Sounder (SSMIS; Kunkee *et al*., 2008) sensor has remained underused due to absolute calibration issues. The Advanced Microwave Scanning Radiometer-Earth Observing System (EOS) (AMSR-E; Kawanishi *et al*., 2003) instrument on the Aqua satellite provides measurements across the microwave spectrum from 6 to 85 GHz at resolutions up to 5 km at the highest frequency. Operational PMW observations useful for precipitation estimation have relied upon the cross-track Advanced Microwave Sounding Unit (AMSU) and MHS instruments that provide information at higher frequencies, between 23.8 and 190 GHz.

In late 1997 the Tropical Rainfall Measuring Mission (TRMM) was launched, the first dedicated precipitation mission (Kummerow *et al*., 1998). The TRMM Precipitation Radar (PR; Iguchi *et al*., 2000) was the first spaceborne precipitation radar and is capable of sampling precipitation both vertically and horizontally to provide 3D images of weather systems. The PR operates at a frequency of 13.6 GHz, optimal for the retrieval of precipitation in the tropics. Although the swath width of the radar is limited to 215 km, the radar is able to retrieve vertical profiles of precipitation from the surface to 20 km every 250 m with a horizontal resolution of 5 km. Meanwhile the SSM/I-like TRMM Microwave Imager (TMI) has provided coincident microwave observations over the Tropics, with the addition of a 10 GHz channel to the SSM/I-like channels for retrieval of heavy precipitation over the oceans. Other instruments on TRMM include the Visible and InfraRed Scanner (VIRS) and the Lightning Imaging Sensor (LIS). The array of instruments on this satellite allows direct comparisons between VIS, IR, passive and active microwave observations. Furthermore, the non-Sun-synchronous nature of TRMM allows samples across the full diurnal cycle to be made as it precesses through the diurnal cycle over a 46 day period.

The exploitation of active microwave observations of precipitation from space has been relatively recent with the TRMM PR being the mainstay of the observations. Despite the fact that the minimal detectable rain rate of the PR is about 0.7 mm h^{-1}, it has proved capable of generating maps of Tropical precipitation (Nesbitt and Anders, 2009). More recently the CloudSat mission launched in 2006 (Stephens *et al*., 2008) has added the Cloud Profiling Radar (CPR) to spaceborne radar observations. This system operates at a frequency of 94 GHz with a resolution along-track of 1.4 km and 480 m vertical range resolution. While it is optimized for observing clouds, the sensor has also proven capable of identifying and retrieving both rainfall and snowfall, and in particular light or very light precipitation (Mitrescu *et al*., 2010).

Improved observations of vertical cloud height, amount and structure are possible due to the Cloud-Aerosol Lidar with Orthogonal Polarization (CALIOP) on the Cloud-Aerosol Lidar and Infrared Pathfinder Satellite Observation (CALIPSO) mission (Winker *et al*., 2007; Hunt *et al*., 2009) together with the Atmospheric InfraRed Sounder (AIRS; Gautier *et al*., 2003). These observations enable better global cloud characterization important for better retrieval of cloud structure and precipitation formation mechanisms (Stubenrauch *et al*., 2007; Kahn *et al*., 2008; Marchand *et al*., 2008; Mace *et al*., 2009).

3. Precipitation retrievals

3.1. VIS/IR methods

Observations made in the VIS and IR parts of the spectrum remain the mainstay of operational meteorological Earth observations. In VIS imagery clouds appear relatively bright against the surface of the Earth due to their high albedo. However, the relationship between cloud brightness and surface precipitation is relatively poor and the imagery is only available during daylight. However, early studies showed that daily rainfall estimates could be derived from available VIS imagery (Follansbee and Oliver, 1975). Despite its limitations, VIS imagery can be used for the delineation of cloud area (and hence regions of no rain) and for identifying types of clouds. Thick clouds, such as cumulonimbus, will reflect more light than thin cirrus clouds, while texture can be used to highlight differences between smooth stratiform clouds and the uneven texture of convective cloud.

Thermal IR imagery depicts the naturally emitted radiation from the Earth's surface and the atmosphere and is therefore available both night and day. In the thermal IR the temperature of clouds, and therefore their heights, can be determined. Through a simple premise that cold clouds rain more than warm clouds, infrared imagery may provide a first-guess rainfall estimate. The relationship between the cloud-top temperatures and rainfall can be established through a statistical relationship

or through dynamic calibration. Early studies included three-hourly estimates from IR (Lethbridge, 1967) and monthly rainfall from nephanalysis (Barrett, 1970). However, the relationship between the cloud top temperature and rainfall is indirect, with significant variations in the relationship occurring during the lifetime of rainfall events, between rain systems and between different climatological regimes. Cold-cloud duration (CCD) techniques have been developed that relate the occurrence of cold clouds to the surface rainfall, such as the Global Precipitation Index (GPI; Arkin, 1979; Arkin and Meisner, 1987). The GPI assigns a constant rain-rate (3 mm h^{-1}) to the fraction of clouds below a set threshold (235 K). Refinements of the GPI include the use of gauge data to adjust the GPI locally (Todd *et al*., 1995, 1999), or through PMW adjustment (e.g. Adler *et al*., 1994; Hsu *et al*., 1999) while the scheme of Todd and Washington (1999) provides adjusted GPI-based precipitation data since 1986 at sub-daily, sub-2.5° resolution. Other IR-based techniques, such as the power-law regression of the Autoestimator (Vicente *et al*., 1998) use an IR : rainfall relationship derived through comparison of collocated satellite radiances with surface radar data. Similar techniques include the revised Autoestimator (Vicente *et al*., 2002) and the Hydroestimator (Kuligowski, 2002). Wu (1991) noted that there was a strong negative correlation between the outgoing long wave radiation (OLR) with precipitation: Xie and Arkin (1998) used this to formulate the OLR Precipitation Index (OPI) to estimate monthly precipitation from polar orbiting satellites. Other examples of IR techniques include Adler and Negri (1988); Anagnostou *et al*. (1999a, 1999b); Grimes *et al*. (1999) and Todd *et al*. (1999), providing useful benchmarks against which to compare other techniques.

Extending the observations into the near InfraRed (nIR), properties of cloud-top particles, such as size and phase, can be obtained from multi-channel data. The use of reflected/emitted radiances around 1.6, 2.1 and 3.9 μm have proved very useful in retrieving the microphysical properties of clouds (Rosenfeld and Gutman, 1994; Rosenfeld and Lensky, 1998). These techniques can be extended to night time through the use of IR temperature differences between the thermal IR 10.8 μm and the 3.7 μm channels (Lensky and Rosenfeld, 2003a, 2003b). The Clouds-Aerosols-Precipitation Satellite Analysis Tool (CAPSAT; Lensky and Rosenfeld, 2008) uses all available VIS/IR channels to classify the imagery using lookup tables tailored to selected microphysical conditions. Thies *et al*. (2008) introduced a method for rain area delineation and rainfall intensity retrieval based on MSG, based upon the assumption that areas with a higher cloud water path and more ice particles in the upper parts are characterized by higher rainfall intensities. Other techniques developed to exploit the multichannel observations of MSG have included Roebeling and Holleman (2009) that uses information on cloud condensed water path (CWP), particle effective radius, and cloud thermodynamic phase to detect precipitating clouds, while CWP and cloud-top height are used to estimate rain rates. Kühnlein *et al*. (2010) also used MSG observations and based their precipitation technique around retrievals of optical thickness and effective particle radius.

Multi-channel techniques initially used dual-channel from VIS and IR imagery (e.g. Lovejoy and Austin, 1979). More recently the GOES Multi-Spectral Rainfall Algorithm (Ba and Gruber, 2001) use the VIS, near IR, water vapour and two thermal IR channels from the GOES satellite to derive rainfall estimates over the U.S. Behrangi *et al*. (2009) have devised a neural network method for improving rain/no rain delineation based on the early work of Hsu *et al*. (1999). Results show that during daytime the VIS 0.65 μm channel improves the rain : no-rain detection when combined with any of the other four GOES-12 channels. At night time two IR channels 6.5 and 10.7 μm improves performance over any single IR channel although the use of more than two channels does not improve the results significantly.

Although the IR techniques have achieved some success in the tropics where convective precipitation systems dominate, in the extra-tropics such techniques are less successful. One notable exception is that based upon the TIROS Operational Vertical Sounder (TOVS) developed by Susskind *et al*. (1997) which uses multiple channels to estimate statistical profiles of temperature and humidity, and fractional cloud cover. These are then processed to generate an estimate of precipitation using an empirical regression that includes latitude, season and surface type.

3.2. Passive microwave methods

Early studies by Savage and Weinman (1975), Weinman and Guetter (1977) and Wilheit *et al*. (1977) investigated measurements from the EMSR-5 and EMSR-6 instruments, relating the observations to calculations of radiative transfer of clouds and rainfall retrieval. This showed that PMW observations were more directly related to precipitation-sized particles than similar observations in the VIS/IR. In the MW part of the spectrum the Earth naturally emits low levels of MW radiation which interacts with precipitation-sized particles in the atmosphere, affecting the received radiation at the sensor. Two distinct processes may be used to identify precipitation. First, emission from rain droplets which leads to an increase in MW radiation and, second, scattering caused by precipitating ice particles which leads to a decrease in received MW radiation. The magnitude of these effects depends upon size and concentration of the particles. However, these processes cannot be observed over all surfaces; over water where the background emissivity (ε) is low ($\varepsilon \sim 0.4–0.5$), the emission from rain drops can be used to quantify the rainfall. Over land surfaces the emissions from rain droplets are masked by the higher and more variable background emissivity ($\varepsilon \sim 0.8–0.9$). Consequently, over land the scattering of the radiation at higher frequencies, caused primarily by ice particles, must be used. Therefore, care is needed in interpreting retrievals over land/ocean regions since different techniques are

used for each region; the emission-based techniques provide a measure of rainfall through the total atmospheric column, whereas scattering-based techniques relate to ice particles in the upper parts of the cloud.

Since the observed PMW brightness temperatures (Tb) generally have a non-unique response to rainfall intensity, multi-channel approaches are the norm. Techniques have been developed to exploit these physical relationships and can be divided in two broad groups: empirically derived and physically derived techniques (see Kidd *et al*., 1998). Empirical techniques are relatively simple to implement and inherently incorporate corrections for artefacts associated with PMW observations (such as beam-filling/inhomogeneous field-of-view, absolute calibration issues, and resolution differences). However, regional calibration is often necessary due to variations in the nature of the different precipitation systems. Dual-channel approaches have proved reasonably successful, relying upon differences between low- and high-frequency observations (Barrett *et al*., 1991) or dual-polarization approaches with the Polarization-Corrected Temperatures (Kidd *et al*., 1988; Spencer *et al*., 1989) to subdue the surface variations and to accentuate the precipitation-related scattering signal. Physical techniques rely upon radiative transfer modelling to interpret the observed radiation, either through the inverse modelling of the observed radiation to retrieve information about the precipitation particles (Smith *et al*., 1992; Mugnai *et al*., 1993), or through the use of *a priori* databases of model-generated atmospheric profiles which are compared with the satellite observations (e.g., Bauer, 2001; Bauer *et al*., 2001). An example of the latter is the Goddard Profiling technique (GPROF; Kummerow *et al*., 2001) which has evolved to ensure consistency between the physical retrievals from the TRMM PR and TMI PMW Tbs through the use of cloud resolving models (Masunaga and Kummerow, 2005). The main advantage of physical techniques is that they provide more information about the precipitation system than just the surface rainfall.

The retrieval of precipitation using PMW observations has always represented a problem over coastal areas; often techniques omit retrievals over the coastline, or use a less optimum technique. Kidd (1998) describes a technique for the delineation and retrieval of rainfall from PMW data using the polarization-corrected temperature (PCT) algorithm, developed from the earlier 'polarization algorithm' concept of Grody (1984). The PCT is able to subdue the effect of background surface emissivities making it possible to delineate areas of rainfall over varying surface types, especially over coastal areas with mixed emissivity signatures from sea, land and combinations of these two. McCollum and Ferraro (2005) implemented the PCT when improving the GPROF V6 algorithm over coastal areas. The availability of high-frequency PMW observations, such as those available from the AMSU-B instrument (Saunders *et al*., 1995), has provided additional PMW frequencies. The higher window (89 and 150 GHz), opaque oxygen (53.6 GHz) and water vapour absorption (183 ± 1, ± 3 and ± 7 GHz) channels of the AMSU-B are impacted less by surface emissivity variations and hence problematic surface backgrounds such as snow/ice and have been used with some success over coastal areas by Kongoli *et al*. (2007).

AMSU-B observations alone can be used to retrieve a number of precipitation-related products including the total precipitable water (Wang and Wilheit, 1989), hydrological parameter (Grody *et al*., 2000); total precipitable water (TPW) and cloud liquid water (CLW) and precipitation over all surfaces (Grody *et al*., 2001; Bennartz *et al*., 2002) and precipitating ice particles (Bennartz and Bauer, 2003). Surussavadee and Staelin (2007) compared histograms of AMSU Tbs with the National Center for Atmospheric Research (NCAR) Mesoscale Model (MM5): this study resulted in a neural network-based technique to retrieve hydrometeor water paths, peak vertical wind, and 15 min average surface precipitation rates for rain and snow, this being critical to extending precipitation retrievals to higher latitudes (Surussavadee and Staelin, 2008a, 2008b).

Laviola and Levizzani (2009) proposed a simple thresholding technique based upon AMSU-B observations. The Water vapour Strong Lines at 183 GHz (183-WSL) algorithm first discriminates between rain and no-rain areas and then retrieves precipitation based upon convective and stratiform regimes. A similar technique by Di Tomaso *et al*. (2009) exploits the 89, 150 and 183 GHz channels where the observed Tbs are analysed though a radiative transfer model for over land and over ocean rainfall retrieval; the probability of detection (POD) of precipitation is 75 and 90% for rain rates greater than 1 and 5 mm h^{-1}, respectively. The inclusion of the AMSU-B data sets, along with the DMSP SSMIS observations, now provides important information in the generation of many precipitation products, in particular those which combine multi-sensor and multi-frequency information.

The main drawback of these PMW based techniques is that observations are currently only available from LEO satellites, typically resulting in two observations per day per satellite. In addition, the resolution of the observations is not ideal: the spatial resolution of the low frequency channels that are used over the ocean is of the order of 50 km $\times$ 50 km, while for the higher-frequency channels used over the land resolutions are typically no better than 10 km $\times$ 10 km. Thus, although the PMW techniques are more direct at detecting and estimating the precipitation, sampling often negates this advantage beyond that of instantaneous retrievals.

3.3. Active microwave methods

Active MW (AMW) techniques offer the most direct of all satellite quantitative estimation methods. Despite this, radar technology for spaceborne precipitation estimation has been limited primarily to the TRMM PR. As with all radar systems, the PR relies upon the interpretation of the backscatter of radiation from the precipitation,

the amount being broadly proportional to the number of precipitation-sized particles. This relationship is not constant, and in heavy precipitation attenuation effects can be significant at the 13.8 GHz frequency of the PR (Iguchi *et al*., 2000). Recently the nadir-only CloudSat CPR (Stephens *et al*., 2008), has provided some significant insights in to precipitation processes and retrieval capabilities. The CPR, operating at 94 GHz, is much more sensitive to cloud hydrometeors but tends to saturate in regions of dense cloud or rainfall. However, through the use of attenuation-correction algorithms and surface reflectivity modelling it can be used in the identification of light rainfall and snowfall. Haynes *et al*. (2009) have demonstrated a notable potential at mid-latitudes over the ocean; the greater sensitivity of the CPR over the TRMM PR has shown a greater occurrence of precipitation over the tropics allowing a more representative distribution function of precipitation intensity to be generated. Improved retrieval techniques highlight the significance of light precipitation, particularly at higher latitudes (Mitrescu *et al*., 2010).

3.4. Multi-sensor techniques

Single-sensor retrievals have the relative advantage of processing simplicity, but the VIS/IR lack the directness of the PMW and the PMW lack the frequency sampling of the VIS/IR. Therefore, to overcome the deficiencies of individual satellite systems a number of techniques have been developed to exploit the combination of different satellite observations. Techniques developed to exploit VIS/IR and PMW observations essentially fall into those that use the PMW to calibrate the IR observations, and those that derive cloud motion from the IR data to move PMW precipitation estimates.

Techniques that generate calibration curves to map IR radiances to other data sets (such as the PMW) are generally termed 'blended' algorithms (e.g. Turk *et al*., 2000; Kidd *et al*., 2003). Most IR-derived estimates can be attributed to this category since even the relatively simple GPI technique was originally determined through the comparison of cold cloud duration to surface data. More advanced techniques include the TRMM Multi-Satellite Precipitation Analysis (TMPA; Huffman *et al*., 2007) which generates a precipitation product at 3-h, 0.25° resolution. This technique ingests data from PMW imagers and sounders, GEO IR data and precipitation gauge analyses for combination into the single precipitation product, as sketched in the next section. Other techniques include the Passive Microwave InfraRed technique (PMIR; Kidd *et al*., 2003), the Microwave-adjusted IR Algorithm (MIRA; Todd *et al*., 2001), the Naval Research Laboratory (NRL) blended technique (Turk *et al*., 2000), the Microwave-Infrared Combined Rainfall Algorithm (MICRA; Marzano *et al*., 2004), the Self-Calibrating Multivariate Precipitation retrieval (SCaMPR; Kuligowski, 2002) and the Microwave/Infrared Rain Rate Algorithm (MIRRA; Miller *et al*., 2001). The use of artificial neural networks (ANNs) have also been investigated. Tapiador *et al*. (2004) describe an ANN technique to generate high temporal and spatial resolution rainfall estimates from both IR and PMW data, while Grimes *et al*. (2003) used an ANN to improve an IR-based cold cloud duration technique with information from a NWP model over Zambia. Hong *et al*. (2005) have routinely adjusted the model parameters of the Precipitation Estimation from Remotely Sensed Information using Artificial Neural Networks (PERSIANN) technique using coincident rainfall derived from the TMI to better represent the diurnal cycle.

Despite some success with the calibrated-IR techniques, they are ultimately limited by the indirectness of the IR to sense the precipitation. However, IR data can be usefully employed to measure cloud movement, which can be used to advect, or morph, the more direct PMW-retrieved precipitation between the successive LEO PMW satellite overpasses. Increasing computer power has enabled the implementation of these real time motion-based (or advection) techniques. Examples of current state-of-the-art methodologies are the Climate Prediction Center Morphing technique (CMORPH; Joyce *et al*., 2004) and the Global Satellite Mapping of Precipitation (GSMaP; Kubota *et al*., 2007). The main drawback of this methodology is that the retrieved cloud motion might not necessarily represent the true motion of the precipitation at the surface, particularly if changes in the surface precipitation pattern occur between the infrequent PMW overpasses. This shortcoming has been addressed to a degree through the Lagrangian Model (LMODEL), proposed by Bellerby *et al*. (2009a, 2009b). This technique is based on a conceptual cloud-development model driven by GEO satellite imagery and is locally updated using PMW-based rainfall measurements from LEO platforms. Single-band thermal IR GEO satellite imagery is used to characterize cloud motion, growth and dispersal at high spatial resolution (4 km) to drive a simple, linear, semi-Lagrangian, conceptual cloud mass balance model, incorporating separate representations of convective and stratiform processes. PMW satellite data updates the model locally using a two-stage process that scales precipitable water fluxes into the model and then updates the model using a Kalman filter.

For many applications the combination of all available data sets is ideal, incorporating products derived from the various satellite observations, gauge data sets and, where available, surface radar data. Various combination schemes have been developed taking account of the expected errors inherent in each of the products: recently, Kalman filters have been used to blend products derived from observations taken from different sources at different times to better account for the errors in the component estimates (Joyce *et al*., 2009; Ushio and Okamoto, 2009; Ushio *et al*., 2009). One multi-source product that is widely used is the Global Precipitation and Climatology Project (GPCP) precipitation product (Huffman *et al*., 1997, Adler *et al*., 2003, Huffman *et al*., 2009), which generates a largely homogeneous global precipitation product. Another dataset

widely used for NWP model verification, climate studies and hydrological applications is the Climate Prediction Center Merged Analysis of Precipitation (CMAP; Xie and Arkin, 1997), which merges satellite IR along with gauge and re-analyses data from the National Centers for Environmental Prediction (NCEP) and NCAR. These are described in detail later.

Other ancillary data may also be used to improve the retrieval of rainfall. Lightning data either from ground based detection networks or from space sensors such as the TRMM LIS or the DMSP Optical Transient Detector (OTD) have been used to pinpoint locations of strong convection. Grecu *et al*. (2000) generated an empirical technique using PMW, IR rainfall estimates and the number of lightning strikes. Results showed a reduction of about 15% in the root-mean-square error of the estimates of rain volumes defined by convective areas associated with lightning. Cecil *et al*. (2005) using TRMM PR, TMI and LIS data over the Tropics and the sub-tropics showed that, even for storms with similar characteristics, storms over water were considerably less likely to produce lightning than comparable storms over land.

One on-going problem for precipitation estimation from space is the estimation of snowfall: snow data are of utmost importance for the closure of the water cycle since on average ∼5% of global annual precipitation falls as snow (ESA, 2004; Levizzani *et al*., 2011). However, the occurrence and accumulation of snow is more significant at higher latitudes: north of 60–70° snowfall dominates the precipitation regimes. Detecting and estimating snowfall over cold, often snow-covered, surfaces is difficult using PMW frequencies below ∼100 GHz. However, at frequencies above 100 GHz water vapour screens the surface emission while the sensitivity to frozen hydrometeors remains significant. Early studies demonstrating the feasibility of snowfall estimation from space using high frequency channels include Liu and Curry (1997), Ferraro *et al*. (2000), Katsumata *et al*. (2000), Staelin and Chen (2000), Weng and Grody (2000), Bennartz and Petty (2001), Wang *et al*. (2001) and Bennartz *et al*. (2002).

The retrieval of snowfall is not straightforward because the radiative properties of snowflakes and ice crystals are much more complex than those of liquid droplets, and because many different types of frozen hydrometeors may co-exist with the precipitating clouds. A number of studies have investigated the radiative properties of frozen hydrometeors. Bennartz and Petty (2001) showed that the variability in the scattering index at 85 GHz was affected by the size of the precipitating ice particles. Evans and Stephens (1995) showed that the particle shape had a significant effect and that at higher frequencies the scattering was essentially independent of the cloud temperature. Liu and Curry (1997) used observations from the SSM/I and Special Sensor Microwave/Temperature-2 (SSM/T2) to identify liquid and frozen precipitation. The main problem is separating the falling from the fallen snow. Bennartz and Bauer (2003) showed that 150 GHz observations were optimal for identifying ice hydrometeors. Below this frequency, the 85 GHz observations were affected too much by the variations in surface emissivity, while the water vapour channels around 183 GHz were affected by environmental conditions. However, the joint exploitation of the 85, 150 and 183 GHz channels is deemed to be an appropriate avenue to investigate further. The combination of the window and water vapour channels provides the means for separating the surface and atmospheric components in the observations. Techniques based upon the 183 GHz channels have shown some success: Laviola and Levizzani (2011) and Surussavadee and Staelin (2010) demonstrated that not only precipitation type and intensity could be retrieved, but that it could be successfully be discriminated from a range of surface backgrounds.

More recently, the availability of CPR data from the CloudSat mission (Stephens *et al*., 2002) has shown great promise in the detection of light precipitation including snowfall. Furthermore, Cloudsat's near polar orbit covers regions that experience snowfall, much more than the TRMM satellite. Development of AMW snowfall retrieval algorithms is still in its infancy, although Liu (2008) showed that a combination of modelled surface temperature and suitable reflectivity-snowfall relationships proved successful. Combined radar-radiometer techniques are also being investigated: Grecu and Olson (2008) outlined a technique for retrieving snowfall over the oceans using Cloudsat and AMSR data. Key to these retrievals however is the ability to represent accurately the habits of the frozen hydrometeors within the physical retrieval schemes.

4. Precipitation products

A good number of precipitation products is available with different spatial and temporal characteristics (Table II). These may be divided into two broad categories, high-resolution precipitation products aimed at the 'operational' user community requiring daily or sub-daily good spatial resolution products, and the long-term climatological data sets that necessitate greater stability, but at the expense of temporal and spatial resolution. There is a number of high resolution precipitation products that generate estimates quasi-globally (60°N to 60°S) at a nominal resolution of 0.25° × 0.25° every 3 h. Key ones are described below.

The TRMM Merged Precipitation Analysis (TMPA; Huffman *et al*., 2007) has three components: the merged microwave product, the microwave-calibrated IR product and the combined microwave-infrared product (3B42), providing routinely generated and distributed precipitation products at 0.25° × 0.25°, 3 h resolution. Data from the TMI, SSM/I and AMSR-E are processed by the Precipitation Processing System (PPS) using the GPROF algorithm (Kummerow *et al*., 1996; Olson *et al*., 1999), while data from the AMSU-B and MHS sensors are processed by National Environmental Satellite, Data, and

Table II. Archive locations for commonly-used precipitation products (see also http://www.isac.cnr.it/~ipwg/algorithms/algorithms-invent.html).

CPC MORPHing technique (CMORPH)
ftp://ftp.cpc.ncep.noaa.gov/precip/global_CMORPH/30_min_8_km
ftp://ftp.cpc.ncep.noaa.gov/precip/global_CMORPH/3-hourly_025deg
ftp://ftp.cpc.ncep.noaa.gov/precip/global_CMORPH/daily_025deg
Global Satellite Mapping of Precipitation (GSMaP)
ftp://hokusai.eorc.jaxa.jp/pub/gsmap_crest/MVK+/hourly
ftp://hokusai.eorc.jaxa.jp/pub/gsmap_crest/MVK+/daily
ftp://hokusai.eorc.jaxa.jp/pub/gsmap_crest/MVK+/monthly
GOES Multispectral Rainfall Algorithm (GMSRA)
http://orbit-net.nesdis.noaa.gov/arad/ht/ff/gmsra.html
GPCP One-Degree Daily (1DD)
http://www1.ncdc.noaa.gov/pub/data/gpcp/1dd/data/
GPCP Satellite-Gauge Combination (SG)
http://lwf.ncdc.noaa.gov/oa/wmo/wdcamet-ncdc.html
NRL Blended Technique
ftp://ftp.nrlmry.navy.mil/pub/receive/turk/global_rain
Precipitation Estimation from Remotely Sensed Information using Artificial Neural Networks (PERSIANN)
http://chrs.web.uci.edu/persiann/
TMPA (3B42)
http://disc.sci.gsfc.nasa.gov/precipitation/documentation/TRMM_README/TRMM_3B42_readme.shtml
Real-Time TMPA (3B42RT)
ftp://trmmopen.gsfc.nasa.gov/pub/merged/mergeIRMicro/

Information System (NESDIS) using the ice-water path technique described by Zhao and Weng (2002) and Weng *et al*. (2003). Where PMW precipitation estimates are not available GEO IR data are used, having been converted to precipitation estimates using a local probability matching between IR Tb and PMW estimates over a month. The 3B42 product is bias-corrected against monthly gauge estimates where available, although an uncorrected version is also available in near-real time. The 3B42 version is available for 1998-present over the latitude band 50°N to 50°S. As well, a near-real-time version is computed (3B42RT), which substitutes a climatological calibration to 3B42 for the final step.

The Climate Prediction Center (CPC) MORPHing (CMORPH) technique exploits the directness of the PMW observations with the cloud motion derived from the IR data (Joyce *et al*., 2004). PMW observations from the AMSU-B, MHS, SSM/I, TMI and AMSR, are used to derive precipitation estimates. The GPROF product (Kummerow *et al*., 1996) is used for the TMI, while the NOAA/NESDIS SSM/I rainfall algorithm (Ferraro, 1997) is used for the SSM/I (see McCollum *et al*., 2002). The ice water path from the AMSU-B is converted to a rain rate using the techniques described by Ferraro *et al*. (2000). The TMI is used as the baseline estimates with AMSU-B estimates scaled to fit. The microwave-only component of the CMORPH technique is termed the CPC Merged Microwave product. IR-derived cloud motion vectors are based upon the correlations between two temporally adjacent images (Purdom and Dills, 1994) with correction factors employed to correct a tendency for the motion to be over-stated Joyce *et al*. (2004). These motion vectors are then used to propagate the PMW-derived rainfall field forwards and backwards in time between the PMW overpasses. The CMORPH product is available at a number of different resolutions to suit end user requirements. An example of the CMORPH product is shown in Figure 3. The data set covers 60°N to 60°S and was recently reprocessed back to 1998 (Xie, personal communication, 2011).

Early studies showed promising results using ANNs: these were able to cope with a range of observations, often with non-linear relationships to the resulting precipitation (Murao *et al*., 1993). The Precipitation Estimation from Remotely Sensed Information using Artificial Neural Networks (PERSIANN) technique was designed to extract and combine information from various sources, such as IR and PMW satellite observations, surface gauges and radar, along with ancillary information such as topography (Hsu *et al*., 1997; Sorooshian *et al*., 2000). Input variables include local IR Tbs (means and standard deviations) and surface type, with calibration against surface data over Japan and Florida. The PERSIANN technique showed that the ANN is capable of deriving good results even with sparse updates, which is ideal for combining the PMW estimates with more frequent and regular IR observations. Estimates are available on the latitude band 60°N to 60°S for 2001-present.

The Passive Microwave-InfraRed (PMIR) technique was devised to combine the information from the PMW and IR data sets through local calibration of the IR Tbs (Kidd *et al*., 2003; Kidd and Muller, 2009). The technique uses data from the SSM/I instrument to derive rain rates from a frequency difference algorithm tuned to surface data sets and the TRMM PR. Co-located and

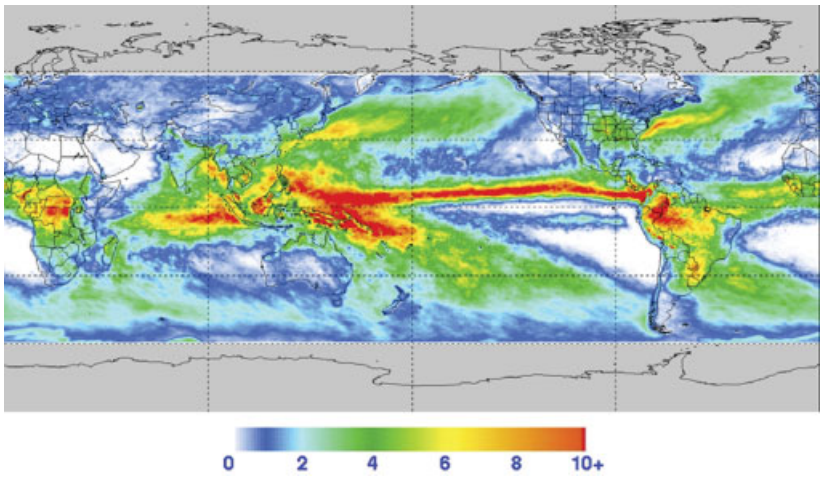

Figure 3. Example of the CMORPH high resolution precipitation product accumulated to show the annual precipitation for 2009, expressed in mm day^{-1}.

co-temporal IR Tbs and PMW observations are entered into a data base for each 1° × 1° gridbox globally, from which cumulative distribution histograms are generated which map the IR Tbs onto the PMW rain rates. The histograms are updated through a temporal/spatial inverse weighting function in one of two ways: a 'climatological' mode where data up to 5 days either side of the current day are used, and a 'real time' mode where only the previous 5 days data are used. Precipitation products are generated at a nominal 12 km, 30 min resolution.

The Naval Research Laboratory (NRL) blended technique is based upon an adaptive analysis of temporally and spatially matched pixels from all available GEO VIS/IR and PMW observations, and TRMM PR (2A25) data (Turk *et al*., 2009) The NRL technique has three stages: collocation of GEO VIS/IR and LEO PMW data to build 2° × 2° lookup tables of IR Tb to PMW rain rates; conversion of IR data into instantaneous rain rates *via* lookup table and; update of accumulations for each 3-h period. Additional corrections are applied based upon model-generated wind vectors for upslope and downslope orographic effects and growth/decay of the clouds based upon the changes in the IR-Tb, are used to intensify or lighten the rain rates (Vicente *et al*., 2002). The baseline product is a global (60°N to 60°S latitude) map of 3-h accumulated precipitation, starting in mid-2000 and updated every 3 h.

The Global Satellite Mapping of Precipitation (GSMaP) product combines precipitation estimates from the TMI, AMSR and SSM/I together with those derived from geostationary IR data (Kubota *et al*., 2007). The technique provides a number of different combination procedures; the MVR version generates cloud motion vectors from the GEO IR data and morphs the PMW rainfall where PMW overpasses are not present; the MVK version uses a Kalman filter approach to generate precipitation estimates in PMW voids. Comparison of the results against surface radar shows correlations of ∼0.8 and low RMSEs. Product generation is at a nominal 0.1° resolution every 30 min. The latitude band covered is 60°N to 60°S for recent time periods that vary by product.

Fully global precipitation products are also available at somewhat coarser time/space resolutions, implicitly aimed at more climate applications.

The suite of GPCP products includes a monthly product (1979–present), a pentad (5 day) analysis (1979–present) and a daily product available for a shorter period (1997–present). Although these three products have been developed separately and using different input data sets and analysis techniques, the higher time resolution products are adjusted to the core monthly analysis, thus giving a consistent set of analyses. The monthly Satellite-Gauge (SG) precipitation analysis is designed to provide a globally complete estimate of surface precipitation at 2.5° × 2.5° latitude–longitude resolution for the period 1979 to the present (Adler *et al*., 2003; Huffman *et al*., 2009), with a temporal consistency that reflects Climate Data Record standards. Prior to mid-1987 the multi-satellite analysis is based on the OPI (Xie and Arkin, 1998). From mid-1987, the technique uses precipitation estimates from the SSM/I and SSMIS to calibrate GEO IR data in the latitude band 40°N to 40°S. At higher latitudes PMW estimates are combined with estimates based on TOVS and AIRS to provide globally complete satellite-only precipitation estimates. These multi-satellite estimates are then combined with the GPCC rain-gauge analyses to correct for large-scale biases. A climatological GPCP product is shown in Figure 4.

The GPCP pentad precipitation analysis provides a nearly globally complete 2.5° × 2.5° set of pentad precipitation fields from 1979–present that is consistent with the GPCP SG monthly. It adjusts the pentad CMAP analysis by the monthly GPCP product so that the overall magnitude of the pentad GPCP matches that of the monthly GPCP while the sub-monthly variability in the pentad CMAP is retained (Xie *et al*., 2003). The 1-Degree Daily (1DD) precipitation analysis provides a global 1° × 1° time series of daily precipitation

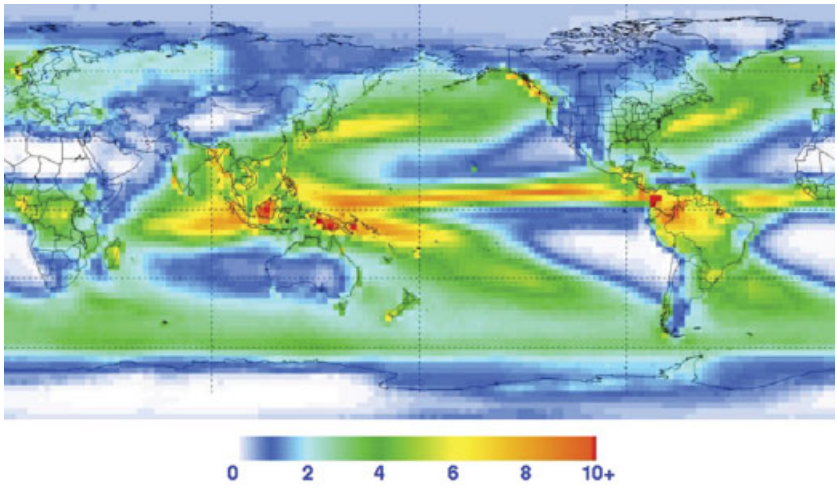

Figure 4. The GPCP satellite-gauge product mean annual precipitation expressed in mm day^{-1}.

fields for October 1996-present that is consistent with the GPCP SG monthly. It uses a Threshold-Matched Precipitation Index (TMPI) in the latitude band 40°N to 40°S to produce instantaneous precipitation from the GEO IR using SSM/I- and SSMIS-derived GPROF estimates of fractional coverage by precipitation to set the T_b threshold. Polewards of 40°S TOVS and AIRS precipitation estimates are adjusted in terms of frequency of precipitation using GPROF at the 40° latitude.

The Climate Prediction Center (CPC) Merged Analysis of Precipitation (CMAP: Xie and Arkin, 1997) provides a precipitation product with full global coverage based on satellite observations (IR, OLR, MSU and PMW), gauge data and model output. The satellite and model estimates are first combined to reduce random errors in the individual data sets. Remaining bias is reduced through comparison with gauge data over land and through a combination of atoll-based gauge data and subjective analysis over the ocean. Xie and Arkin note that the resulting product showed little discontinuity in time-series analysis despite the range of different sensors used. Comparison with the existing Jaeger (1976) and Legates and Willmott (1990) climatologies were good except over the oceans, particularly in the eastern Pacific. Comparisons with the GPCP product, although agreeing well over land, over the tropical oceans greater differences were apparent while significant differences were found in the extra-tropical regions; this was attributed to the input data sets and the handling of biases and errors of the input data. The CMAP product was extended further to a 23 year record (Xie *et al*., 2003) with the adjustment of the CMAP observation-only pentad product to the GPCP merged-analysis to ensure consistency on a monthly scale. A comparison by Yin *et al*. (2004) found that the GPCP produced greater precipitation in the high latitudes compared to the CMAP technique, and that the GPCP also produced more reasonable results over the oceans: differences between the results were attributed to the input data sets and the different merging methodologies. They did however caution against the use of the data sets for long-term trend analysis since some of the identified trends were related to availability of data sets used in the analysis.

One notable ocean-only product is that produced by the Hamburg Ocean Atmosphere Parameters and fluxes from Satellite data (HOAPS; Anderson *et al*., 2011). The data set is based upon observations from the SSM/I instrument with inter-sensor calibration between the different SSM/I sensors to ensure continuity for subsequent time series analysis. The precipitation product is based upon a neural network using European Centre for Medium-Range Weather Forecasts (ECMWF) modelled precipitation to train the network: only SSM/I observations are used, although SSMIS are now being incorporated. Comparison of the HOAPS with GPCP shows that the HOAPS precipitation product produces generally more precipitation in the eastern Pacific and south of Japan, although the overall global values are similar. Both the HOAPS and GPCP product suggest less precipitation than that generated by the ERA-Interim reanalysis product (Anderson *et al*., 2011).

5. Precipitation product performance

A number of inter-comparison projects have been undertaken to evaluate the performance of precipitation estimates derived from satellite observations and models. The NASA WetNet project (Dodge and Goodman, 1994) organized a series of Precipitation Inter-comparison Projects (PIP) concentrating on global monthly estimates (PIP-1 and PIP-3; Barrett *et al*., 1994a, 1994b; Kniveton *et al*., 1994; Adler *et al*., 2001) and regional-scale performance (PIP-2; Smith *et al*., 1998). Alongside these studies the Global Energy and Water Cycle Experiment (GEWEX)/GPCP Algorithm Inter-comparison Programme (AIP) studied product performance over targeted regions (Arkin and Xie, 1994; Ebert *et al*., 1996; Ebert and Manton, 1998). The main conclusion from the PIP and AIP studies was that PMW techniques were clearly better than IR techniques for instantaneous estimates,

primarily due to more direct observation of rainfall. This advantage deteriorated over longer time scales due to poorer sampling inherent in the PMW observations compared with the IR-based techniques. The combined IR-PMW techniques, which were very much in the infancy at this time, did not show a clear advantage at this stage over the IR-alone techniques. Some of the limited success of the combined techniques could be attributed to shortcomings in the component data sets whose errors propagate through to the final product. Overall, it was noted that no single technique or methodology could be deemed superior to any other since all algorithms were affected to differing degrees on common underlying factors, such as surface background conditions, seasons/latitude and meteorological conditions.

Currently, the International Precipitation Working Group (IPWG) provides a focus for operational and research satellite-based quantitative precipitation measurement issues and challenges, addressing a number of key objectives and recommendation (Turk and Bauer, 2006; Kidd *et al*., 2010). It provides a forum for the exchange of information on methods for measuring precipitation and their impact on numerical weather prediction, hydrometeorology and climate studies. The IPWG currently provides on-going near real time validation of quasi-operational and operational satellite estimates, as well as NWP model outputs (see Ebert *et al*., 2007). Intercomparison regions have been established to provide quantitative information on the performance of satellite rainfall products in near real-time to algorithm developers, and the wider user community. The current regional sites include US, Europe, Australia, Japan and South America, using radar and/or gauge data as their surface ground truth. Other validation efforts over South Korea, China, South Africa and Ethiopia provide supporting limited studies. These results show that the NWP models and motion-based techniques outperform the standard satellite estimates of precipitation in cold-season environments (e.g. during mid-latitude winters). However, warm-season performance studies tend to favour the satellite techniques since these can capture the convective nature of the precipitation better than existing NWP models (e.g., Ebert *et al*., 2007).

An offshoot of the IPWG activities has been the establishment of the Program for the Evaluation of High-Resolution Precipitation Products (PEHRPP) to help characterize the errors in high-resolution precipitation products (HRPPs), with $0.25^\circ \times 0.25^\circ$, three hourly resolution or less, over different spatial, temporal, regional and climate scales (see Turk *et al*., 2008). Sapiano and Arkin (2009) compared the CMORPH, TMPA, NRL and PERSIANN HRPPs over the US Southern Great Plains site (in Oklahoma/Kansas) and over the Pacific Ocean from 2003 to 2006. Over land, product : gauge correlations were generally better during warm season, with CMORPH producing the highest correlations. All products had a small positive bias during winter, whereas in summer CMORPH, NRL and PERSIANN had $\sim$100% positive bias, attributed to the over-estimation of convective events. Over the ocean techniques generally underestimated the precipitation, particularly over the eastern Pacific region (east of 150 °W). In another study, Sohn *et al*. (2010) compared HRPPs over the Korean Peninsula (33–39°N, 125–130 °E) using a dense network of 520 gauges. The TMPA, CMORPH, PERSIANN and NRL, together with the 2A12 product from the TMI were selected over summer (rainy) season (JJA) from 2003 to 2006. The TMPA performed best since it incorporates gauge information into the final product. It was noted however that the TMI product, used as the input into the selected HRPP techniques, significantly underestimated the precipitation. These results were echoed by Kidd *et al*. (in press) in a study over NW Europe. Comparison with surface radar and gauge networks showed that above 35°N the satellite-only precipitation products underestimated the precipitation primarily because they are tuned to the TMI product that underestimated the precipitation. Seasonally, the satellite products performed best during the summer months, producing correlations up to about 0.8. The ECMWF operational forecast model was deemed best overall, although it was out-performed by the satellite techniques during the summer.

A common theme in many of the inter-comparison and validation studies is that of error characterization, not least because it is recognized that no single technique or surface data set is error-free. The relative contributions of error from different satellite sensors were studied by Huffman *et al*. (1997) as part of the GPCP combined precipitation product. Krajewski *et al*. (2000) investigated reference sites to quantify the error variance at monthly time scales, while other studies have concentrated on the assessment of error in daily products (Gebremichael and Krajewski, 2005; McPhee and Margulis, 2005). Bowman (2005) studied the spatial and temporal averaging errors of the TRMM precipitation retrievals and ocean gauge data over the tropical Pacific Ocean, while other validation studies clustered around the TRMM products, either using the TRMM ground validation sites or independent datasets, including Nicholson *et al*. (2003a, 2003b), Nesbitt *et al*. (2004), Wolff *et al*. (2005) and Marks *et al*. (2009).

Bellerby and Sun (2005) developed a methodology to assess the uncertainties in IR/PMW satellite precipitation products, deriving conditional probability distribution functions of rainfall on a pixel-by-pixel basis. A simple model of the spatial-temporal covariance structure of the uncertainty in the precipitation field was then used to stochastically generate an ensemble precipitation product. Similar studies by Hossain and Anagnostou (2006a, 2006b) investigated the ensemble generation of satellite rainfall products by a multidimensional satellite rainfall error model with the aim of characterizing the multidimensional stochastic error structure of satellite rainfall estimates as a function of scale. An example application of error characterization is in the assimilation of precipitation estimates into hydrological models, and in particular,

studying the propagation of such errors in such models (Hossain and Anagnostou, 2004; Hossain *et al*., 2004).

Long-term precipitation estimates are now available that permit the study of regional-scale precipitation systems on an inter-annual basis, including studies into monsoon regimes over regions such as North America (Gebremichael *et al*., 2007) and Taiwan and the Far East (Wang and Chen, 2008). Regional climatological studies have included tropical South America (De Angelis *et al*., 2004) and the tropical East Pacific (Cifelli *et al*., 2008). The availability of multi-year sub-daily rainfall data derived from satellite observations have enabled the study of diurnal cycles across the globe, and in particular over the Tropics (Nesbitt and Zipser, 2003, Yang and Smith, 2006).

6. Conclusions and future directions

Precipitation products derived from satellite observations have now reached a good level of maturity with ongoing research and development to improve the accuracy and the resolution (temporal and spatial) of these products. In part, this level of maturity is due to the relatively data-rich environment for satellite rainfall estimates; VIS and IR data derived from GEO satellites is available nominally every 30 min, while a good number of PMW instruments (imagers and sounders) are currently available, providing an average sampling interval <3 h. However, further work is needed to continue to develop error estimates that are vital to hydrological modelling and water resource assessment.

The future development of quantitative precipitation estimates from satellite observations involves both the continuation of operational missions for hydrometeorological applications and utilization/exploitation of long term data sets critical for climate monitoring (Asrar *et al*., 2001). Operational missions envisage the continuation of the European MetOp LEO satellite with improved capabilities, while plans are currently underway for a transition of the U.S. NOAA and DMSP LEO satellite series to Joint Polar Satellite Series (JPSS) and Defense Weather Satellite Series, launch of the Korean Communication, Ocean, and Meteorological Satellite (COMS; http://web.kma.go.kr/eng/about/abo_03_04.jsp), continuation of the Japanese MT-Sat series, and a transition to EUMETSAT's Meteosat Third Generation (MTG) satellites (Stuhlmann *et al*., 2005) and the U.S. GOES-R series (Schmit *et al*., 2005). Research and development missions such as the U.S. NPOESS Preparatory Project satellite, the Japanese Global Change Observation Mission (GCOM) with an AMSR-like instrument, the French-Indian Megha-Topiques mission and the European Space Agency's (ESA) Clouds, Aerosol and Radiation Explorer (EarthCARE) will provide additional data sets that will enhance the current observational capabilities for precipitation retrieval.

The most important upcoming mission for global precipitation mapping is centred on the Global Precipitation Measurement (GPM) mission lead by NASA and the Japan Aerospace Exploration Agency (JAXA), the core satellite of which is due for launch in 2013 (Hou *et al*., 2008). This mission has been identified by the Committee on Earth Observation Satellites (CEOS) as a prototype of the Global Earth Observation System of Systems (GEOSS). GPM consists of a core satellite with the GPM Microwave Imager (GMI; http://gpm.gsfc.nasa.gov/gmi.html) covering a frequency range between 10 and 183 GHz and the dual-wavelength precipitation radar (DPR, Nakamura *et al*., 2005) consisting of a Ku-band precipitation radar (KuPR, 13.6 GHz) and a Ka-band precipitation radar (KaPR, 35.5 GHz). Additional satellites will be provided by international partners, and together with operational satellites, will help ensure temporal sampling of 3 h or less. Coupled with the satellite effort, new techniques are being developed to combine satellite observations into standard and comparable measurements to ensure consistency across the different constellation sensors. Alongside the satellite missions substantial surface validation efforts using ground-based and airborne radars are being organized to ensure maximum use of the satellite observations (Grecu and Anagnostou, 2004; Nakamura and Iguchi, 2007).

Future missions with new technologies are being planned with the potential to improve precipitation retrievals. In particular, the identification and retrieval or frozen precipitation is crucial to improved precipitation retrievals for truly global precipitation estimates. Concepts for missions capable of improved snowfall measurements are being devised using multi-frequency radar, such as 35 and 94 GHz, alongside high-frequency passive microwave radiometers. Other studies have looked at new orbital concepts such as the deploying mini-satellites into elliptical orbits (FLORAD; Marzano *et al*., 2009, 2010) using mm-wave scanning radiometers. The possibilities of geostationary PMW observations have been also studied through the use of synthetic aperture antennas to overcome the diffraction limits of existing systems (e.g. Lambrigtsen *et al*., 2007), although the initial designs of such systems rely upon very high frequencies that respond to precipitation less directly.

Critical to the ongoing use and exploitation of future observations is the availability of high quality satellite data sets in near real time, including the merged global IR composite (Janowiak *et al*., 2001) which is a fundamental input into many quasi-global techniques. As well, permanent archives and episodic reprocessing are also needed to ensure long-term usability of the data sets and improvements to precipitation products. Indeed, not just satellite data, but also data from models and data from non-precipitation missions that can provide additional information for retrieval methodologies and techniques. Improved radiative transfer modelling and the combined use of both active and passive observations (e.g. CPR, AMSR-E and AMSU-B) will help, although the sensitivity to shallow precipitation remains an issue, particularly over highly variable surface backgrounds (Huffman *et al*., 2011). The precipitation products, data and software require wider dissemination to ensure that they are

fully used. As part of this effort, it is important for user training to be increased, and for the precipitation products to be integrated into end-to-end applications that non-expert users can apply more easily.

Acronyms

AIP Algorithm Intercomparison Project
AIRS Atmospheric InfraRed Sounder
AMSR-E Advanced Microwave Scanning Radiometer-Earth Observing System (EOS)
AMSU-B Advanced Microwave Sounding Unit-B
ANN Artificial Neural Network
AVHRR Advanced Very High Resolution Radiometer
CALIOP Cloud-Aerosol Lidar with Orthogonal Polarization
CALIPSO Cloud-Aerosol Lidar and Infrared Pathfinder Satellite Observation
CAPSAT Clouds-Aerosols-Precipitation Satellite Analysis Tool
CCD Cold Cloud Duration
CLW Cloud Liquid Water
CMAP Climate Prediction Center Merged Analysis of Precipitation
CMORPH Climate Prediction Center Morphing algorithm
COMS Communication, Ocean, and Meteorological Satellite
CPR Cloud Profiling Radar
CWP Condensed Cloud Water Path
DMSP Defense Meteorological Satellite Program
DPR Dual-wavelength precipitation radar
DWSS Defense Weather Satellite System
EarthCARE Earth Clouds, Aerosol and Radiation Explorer
ECMWF European Center for Medium Range Weather Forecasting
ESA European Space Agency
ESMR Electrically Scanning Microwave Radiometer
EUMETSAT European Organisation for the Exploitation of Meteorological Satellites
GCOM Global Change Observation Mission
GEO Geostationary
GEWEX Global Energy and Water Cycle Experiment
GHCN Global Historical Climatology Network
GMI GPM Microwave Imager
GOES Geostationary Operational Environmental Satellite
GOS Global Observing System
GPCC Global Precipitation Climatology Centre
GPCP Global Precipitation Climatology Project
GPI GOES Precipitation Index
GPM Global Precipitation Measurement
GPROF Goddard Profiling algorithm
GSMaP Global Satellite Mapping of Precipitation
GTS Global Telecommunication System
HOAPS Hamburg Ocean Atmosphere Parameters and fluxes from Satellite data
HRPP High-resolution precipitation product
IPCC Intergovernmental Panel on Climate Change
IPWG International Precipitation Working Group
IR InfraRed (Thermal)
JAXA Japan Aerospace Exploration Agency
JPSS Joint Polar Satellite System
LEO Low Earth Orbiting
LIS Lightning Imaging Sensor
LMODEL Lagrangian Model
MetOp Operational Meteorological satellite
MHS Microwave Humidity Sounder
MICRA Microwave-Infrared Combined Rainfall Algorithm
MIRA Microwave-adjusted IR Algorithm
MIRRA Microwave/Infrared Rain Rate Algorithm
MM5 Mesoscale Model 5
MODIS Moderate-Resolution Imaging Sensor
MSG Meteosat Second Generation
MSU Microwave Sounding Unit
MTG Meteosat Third Generation
MTSAT Multifunctional Transport Satellite
MW Microwave
NASA National Aeronautics and Space Administration
NESDIS National Environmental Satellite and Data Information Service
NCAR National Center for Atmospheric Research
NOAA National Oceanic and Atmospheric Administration
NWP Numerical Weather Prediction
nIR Near InfraRed
NRL Naval Research Laboratory
OLR Outgoing Long wave Radiation
OPI OLR Precipitation Index
OTD Optical Transient Detector
PCT Polarization Corrected Temperature
PEHRPP Program for the Evaluation of High-Resolution Precipitation Products
PERSIANN Precipitation Estimation from Remotely Sensed Information using Artificial Neural Networks
PIP Precipitation Intercomparison Project
PMIR Passive Microwave InfraRed
PMW Passive microwave
PPS Precipitation Processing System
PR Precipitation Radar
PW PetaWatts (10^{15} W)
SEVIRI Spinning Enhanced Visible and Infrared Imager
SMMR Scanning Multichannel Microwave Radiometer
SSMIS Special Sensor Microwave Imager-Sounder
SSM/I Special Sensor Microwave/Imager
SSM/T2 Special Sensor Microwave/Temperature-2
Tb Brightness temperature
TIROS Television InfraRed Observing Satellite
TMI TRMM Microwave Imager
TMPA TRMM Multi-satellite Precipitation Analysis
TMPI Threshold-Matched Precipitation Index
TOVS TIROS Operational Vertical Sounder

TPW Total Precipitable Water
TRMM Tropical Rainfall Measuring Mission
VIRS Visible and InfraRed Scanner
VIS Visible
WMO World Meteorological Organisation

References

Adler RF, Huffman GJ, Chang A, Ferraro R, Xie P, Janowiak J, Rudolf B, Schneider U, Curtis S, Bolvin D, Gruber A, Susskind J, Arkin P, Nelkin E. 2003. The version-2 Global Precipitation Climatology Project (GPCP) monthly precipitation analysis (1979–Present). *Journal of Hydrometeorology* **4**: 1147–1167.

Adler RF, Huffman GJ, Keehn PR. 1994. Global tropical rain estimates from microwave-adjusted geosynchronous IR data. *Remote Sensing Reviews* **11**: 125–152.

Adler RF, Kidd C, Petty G, Morrissey M, Goodman HM. 2001. Intercomparison of global precipitation products: the third Precipitation Intercomparison Project (PIP-3). *Bulletin of the American Meteorological Society* **82**: 1377–1396.

Adler RF, Negri AJ. 1988. A satellite infrared technique to estimate tropical convective and stratiform rainfall. *Journal of Applied Meteorology* **27**: 30–51.

Anagnostou EN, Krajewski WF, Smith J. 1999a. Uncertainty quantification of mean-areal radar-rainfall estimates. *Journal of Atmospheric and Oceanic Technology* **16**: 206–215.

Anagnostou EN, Negri AJ, Adler RF. 1999b. A satellite infrared technique for diurnal rainfall variability studies. *Journal of Geophysical Research* **104**: 31477–31488.

Anderson A, Klepp C, Fennig K, Bakan S, Grassl H, Schulz J. 2011. Evaluation of the HOAPS-3 ocean surface freshwater flux components. *Journal of Applied Meteorology and Climatology* **50**: 379–398.

Arkin P. 1979. Relationship between fractional coverage of high cloud and rainfall accumulations during GATE over the B-Scale array. *Monthly Weather Review* **107**: 1382–1387.

Arkin PA, Meisner BN. 1987. The relationship between large-scale convective rainfall and cold cloud over the western hemisphere during 1982–1984. *Monthly Weather Review* **115**: 51–74.

Arkin PA, Xie P. 1994. The Global Precipitation Climatology Project: first algorithm intercomparison project. *Bulletin of the American Meteorological Society* **75**: 401–419.

Asrar G, Kaye JA, Morel P. 2001. NASA research strategy for earth system science: climate component. *Bulletin of the American Meteorological Society* **82**: 1309–1329.

Ba MB, Gruber A. 2001. GOES multispectral rainfall algorithm (GMSRA). *Journal of Applied Meteorology* **40**: 1500–1514.

Barrett EC. 1970. The estimation of monthly rainfall from satellite data. *Monthly Weather Review* **98**: 322–327.

Barrett EC, Adler RF, Arpe K, Bauer R, Berg W, Chang A, Ferraro R, Ferriday J, Goodman S, Hong Y, Janowiak J, Kidd C, Kniveton D, Morrissey M, Olson W, Petty G, Rudolf B, Shibata A, Smith E, Spencer R. 1994b. The first WetNet Precipitation Inter-comparison Project: interpretation of results. *Remote Sensing Reviews* **11**: 303–373.

Barrett EC, Dodge J, Goodman HM, Janowiak J, Kidd C, Smith EA. 1994a. The first WetNet Precipitation Intercomparison Project. *Remote Sensing Reviews* **11**: 49–60.

Barrett EC, Kidd C. 1991. The mapping and monitoring of rainfall and other key environmental variables by the SSM/I: some global and regional results. Final Report (stage II) Universities Space Research Association: Columbia, MD; 79.

Barrett EC, Kidd C, Bailey JO. 1988. The special sensor microwave/imager: a new instrument with rainfall monitoring potential. *International Journal of Remote Sensing* **9**: 1943–1950.

Bauer P. 2001. Over-ocean rainfall retrieval from multi-sensor data of the Tropical Rainfall Measuring Mission (TRMM)-Part I: development of inversion databases. *Journal of Atmospheric and Oceanic Technology* **18**: 1315–1330.

Bauer P, Amayenc P, Kummerow CD, Smith EA. 2001. Over-ocean rainfall retrieval from multisensory data or the Tropical Rainfall Measuring Mission. Part II: algorithm implementation. *Journal of Atmospheric and Oceanic Technology* **18**: 1838–1855.

Behrangi A, Hsu K-L, Imam B, Sorooshian S, Kuligowski R. 2009. Evaluating the utility of multispectral information in delineating the areal extent of precipitation. *Journal of Hydrometeorology* **10**: 684–700.

Bellerby T, Hsu K-L, Sorooshian S. 2009a. LMODEL: a satellite precipitation methodology using cloud development modeling. Part I: algorithm construction and calibration. *Journal of Hydrometeorology* **10**: 1081–1095.

Bellerby T, Hsu K-L, Sorooshian S. 2009b. LMODEL: a satellite precipitation methodology using cloud development modeling. Part II: validation. *Journal of Hydrometeorology* **10**: 1096–1108.

Bellerby TJ, Sun J. 2005. Probabilistic and ensemble representations of the uncertainties in an IR/microwave satellite precipitation product. *Journal of Hydrometeorology* **6**: 1032–1044.

Bennartz R, Bauer P. 2003. Sensitivity of microwave radiances at 85–183 GHz to precipitating ice particles. *Radio Science* **38**: 8075, DOI: 8010.1029/2002RS002626.

Bennartz R, Petty GW. 2001. The sensitivity of microwave remote sensing observations of precipitation to ice particle size distributions. *Journal of Applied Meteorology* **40**: 345–364.

Bennartz R, Thoss A, Dybbroe A, Michelson D. 2002. Precipitation analysis using the Advanced Microwave Sounding Unit in support of nowcasting applications. *Meteorological Applications* **9**: 177–189.

Bowman KP. 2005. Comparison of TRMM precipitation retrievals with rain gauge data from ocean buoys. *Journal of Climate* **18**: 178–190.

Bringi VN, Tang T, Chandrasekar V. 2004. Evaluation of a new polarimetrically based Z–R relation. *Journal of Atmospheric and Oceanic Technology* **21**: 612–623.

Cecil DJ, Goodman SJ, Boccippio DJ, Zipser EJ, Nesbitt SW. 2005. Three years of TRMM precipitation features. Part I: radar, radiometric, and lightning characteristics. *Monthly Weather Review* **133**: 543–566.

Cifelli R, Nesbitt SW, Rutledge SA, Petersen WA, Yuter S. 2008. Diurnal characteristics of precipitation features over the Tropical East Pacific: a comparison of the EPIC and TEPPS regions. *Journal of Climate* **21**: 4068–4086.

Dai A, Fung I, Del Genio A. 1997. Surface observed global land precipitation variations during 1900–1998. *Journal of Climate* **11**: 2943–2962.

Dai A, Trenberth KE. 2002. Estimates of freshwater discharge from continents: latitudinal and seasonal variations. *Journal of Hydrometeorology* **3**: 660–687.

De Angelis CF, McGregor GR, Kidd C. 2004. A 3 year climatology of rainfall characteristics over tropical and subtropical South America based on tropical rainfall measuring mission precipitation radar data. *International Journal of Climatology* **24**: 385–399.

Di Tomaso E, Romano F, Cuomo V. 2009. Rainfall estimation from satellite passive microwave observations in the range 89 GHz to 190 GHz. *Journal of Geophysical Research* **114**: D18203, DOI: 10.1029/2009JD011746.

Dodge J, Goodman HM. 1994. The WetNet project. *Remote Sensing Reviews* **11**: 5–21.

Ebert EE, Janowiak JE, Kidd C. 2007. Comparison of near-real-time precipitation estimates from satellite observations and numerical models. *Bulletin of the American Meteorological Society* **88**: 47–64.

Ebert EE, Manton MJ. 1998. Performance of satellite rainfall estimation algorithms during TOGA COARE. *Journal of Atmospheric Science* **55**: 1537–1557.

Ebert EE, Manton MJ, Arkin PA, Allam RJ, Holpin GE, Gruber A. 1996. Results from the GPCP Algorithm Intercomparison Programme. *Bulletin of the American Meteorological Society* **77**: 2875–2887.

ESA 2004. EGPM – European Contribution to Global Precipitation Measurement, ESA SP-1279(5), ESA: Noordwijk, the Netherlands; 60. http://esamultimedia.esa.int/docs/SP_1279_5_EGPM.pdf (accessed 9 August 2011).

Evans KF, Stephens GL. 1995. Microwave radiative transfer through clouds composed of realistically shaped ice crystals. Part II: remote sensing of ice clouds. *Journal of Atmospheric Science* **52**: 2058–2072.

Ferraro RR. 1997. Special sensor microwave imager derived global rainfall estimates for climatological applications. *Journal of Geophysical Research, Atmospheres* **102**: 16715–16735.

Ferraro RR, Weng F, Grody NC, Zhao L. 2000. Precipitation characteristics over land from the NOAA-15 AMSU sensor. *Geophysical Research Letters* **27**: 2669–2672.

Follansbee WA, Oliver VJ. 1975. *A Comparison of Infrared Imagery and Video Pictures in the Estimation of Daily Rainfall from Satellite Data*. Technical Memo. NESS 62, NOAA. National Environmental Satellite Services: Washington, DC; 14.

Fritz S, Wexler H. 1960. Cloud pictures from satellite TIROS I. *Monthly Weather Review* **88**: 79–87.

Gautier C, Shiren Y, Hofstadter M. 2003. AIRS/Vis near IR instrument. *IEEE Transactions on Geoscience and Remote Sensing* **41**: 330–342.

Gebremichael M, Krajewski WF. 2005. Effect of temporal sampling on inferred rainfall spatial statistics. *Journal of Applied Meteorology* **44**: 1626–1633.

Gebremichael M, Vivoni ER, Watts CJ, Rodriguez JC. 2007. Submesoscale spatiotemporal variability of North American monsoon rainfall over complex terrain. *Journal of Climate* **20**: 1751–1773.

Goodrum G, Kidwell KB, Winston W. 2000. NOAA KLM User's Guide with NOAA-N, N' Supplement. http://www2.ncdc.noaa.gov/docs/klm/index.htm (retrieved 11 May 2011).

Grecu M, Anagnostou EN. 2004. A differential attenuation based algorithm for estimating precipitation from dual-wavelength spaceborne radar. *Canadian Journal of Remote Sensing* **30**: 697–705.

Grecu M, Anagnostou EN, Adler RF. 2000. Assessment of the use of lightning information in satellite infrared rainfall estimation. *Journal of Hydrometeorology* **1**: 211–221.

Grecu M, Olson WS. 2008. Precipitating snow retrievals from combined airborne cloud radar and millimeter-wave radiometer observations. *Journal of Applied Meteorology and Climatology* **47**: 1634–1650.

Grimes DIF, Coppola E, Verdecchia M, Visconti G. 2003. A neural network approach to real-time rainfall estimation for Africa using satellite data. *Journal of Hydrometeorology* **4**: 1119–1133.

Grimes DIF, Pardo-Iguzquiza E, Bonifacio R. 1999. Optimal areal rainfall estimation using raingauges and satellite data. *Journal of Hydrology* **222**: 93–108.

Grody NC. 1984. Precipitation monitoring over land from satellites by microwave radiometry. *Proceedings of the IGARSS'84 Symposium*, 27–30 August 1984, Strasbourg.

Grody NC, Weng F, Ferraro RR. 2000. Application of AMSU for obtaining hydrological parameters. In *Microwave Radiometry and Remote Sensing of the Earth's Surface and Atmosphere*, Pampaloni P, Paloscia S (eds). VSP International Science Publications: Utrecht; 339–352.

Grody NC, Zhao J, Ferraro RR. 2001. Determination of precipitable water and cloud liquid water over oceans from the NOAA 15 advanced microwave sounding unit. *Journal of Geophysical Research* **106**: 2943–2953.

Haynes JM, L'Ecuyer TS, Stephens GL, Miller SD, Mitrescu C, Wood NB, Tanelli S. 2009. Rainfall retrieval over the ocean with spaceborneW-band radar. *Journal of Geophysical Research* **114**: D00A22, DOI: 10.1029/2008JD009973.

Hong Y, Hsu K-L, Sorooshian S, Gao X. 2005. Improved representation of diurnal variability of rainfall retrieved from the Tropical Rainfall Measurement Mission Microwave Imager adjusted Precipitation Estimation From Remotely Sensed Information Using Artificial Neural Networks (PERSIANN) system. *Journal of Geophysical Research* **110**: D06102, DOI: 06110.01029/02004JD005301.

Hossain F, Anagnostou EN. 2004. Assessment of current passive-microwave- and infrared-based satellite rainfall remote sensing for flood prediction. *Journal of Geophysical Research* **109**: D07102, DOI: 07110.01029/02003JD003986.

Hossain F, Anagnostou EN. 2006a. Assessment of a multidimensional satellite rainfall error model for ensemble generation of satellite rainfall data. *IEEE Transactions on Geoscience Remote Sensing Letters* **3**: 419–423.

Hossain F, Anagnostou EN. 2006b. A two-dimensional satellite rainfall error model. *IEEE Transactions on Geoscience Remote Sensing* **44**: 1511–1522.

Hossain F, Anagnostou EN, Dinku T. 2004. Sensitivity analyses of satellite rainfall retrieval and sampling error on flood prediction uncertainty. *IEEE Transactions on Geoscience Remote Sensing* **42**: 130–139.

Hou AY, Skofronick-Jackson G, Kummerow CD, Shepherd JM. 2008. Global precipitation measurement. In *Precipitation: Advances in Measurement, Estimation and Prediction*, Michaelides S (ed.). Springer: Berlin; 131–169.

Hsu K, Gao X, Sorooshian S, Gupta HV. 1997. Precipitation estimation from remotely sensed information using artificial neural networks. *Journal of Applied Meteorology* **36**: 1176–1190.

Hsu KL, Gupta HV, Gao XG, Soorshian S. 1999. Estimation of physical variables from multichannel remotely sensed imagery using a neural network: application to rainfall estimation. *Water Resources and Research* **35**: 1605–1618.

Huffman GJ, Adler RF, Arkin P, Chang A, Ferraro R, Gruber A, Janowiak J, McNab A, Rudolf B, Schneider U. 1997. The Global Precipitation Climatology Project (GPCP) combined precipitation dataset. *Bulletin of the American Meteorological Society* **78**: 5–20.

Huffman GJ, Adler RF, Bolvin DT, Gu G. 2009. Improving the global precipitation record: GPCP Version 2.1. *Geophysical Research Letters* **36**: L17808, DOI: 10.1029/2009GL040000.

Huffman GJ, Adler RF, Bolvin DT, Gu G, Nelkin EJ, Bowman KP, Hong Y, Stocker EF, Wolff DB. 2007. The TRMM Multisatellite Precipitation Analysis (TMPA): quasiglobal, multiyear, combined-sensor precipitation estimates at fine scales. *Journal of Hydrometeorology* **8**: 38–55.

Huffman GJ, Klepp C. 2011. Meeting Summary: Fifth Workshop of the International Precipitation Working Group. *Bulletin of the American Meteorological Society* (in press).

Hulme M. 1994. Validation of large-scale precipitation fields in General Circulation Models. In *Global Precipitation and Climate Change*, Debois M, Desalmand F (eds). Springer: Berlin; 387–405.

Hunt WH, Winker DM, Vaughan MA, Powell KA, Lucker PL, Weimer C. 2009. CALIPSO lidar description and performance assessment. *Journal of Atmospheric and Oceanic Technology* **26**: 1214–1228.

Iguchi T, Kozu T, Meneghini R, Awaka J, Okamoto K. 2000. Rain-profiling algorithm for the TRMM precipitation radar. *Journal of Applied Meteorology* **39**: 2038–2052.

IPCC. 2007. *Contribution of Working Group I to the Fourth Assessment Report of the Intergovernmental Panel on Climate Change*, Solomon S, Qin D, Manning M, Chen Z, Marquis M, Averyt KB, Tignor M, Miller HL (eds). Cambridge University Press: Cambridge, New York, NY.

Jaeger L. 1976. Monatskarten des Neiderschiags fur die ganze Erde. Berichte des Deutscher Wetterdientes, Offenbach; 33 and plates.

Janowiak JE, Joyce RJ, Yarosh Y. 2001. A real-time global half-hourly pixel-resolution infrared dataset and its applications. *Bulletin of the American Meteorological Society* **82**: 205–217.

Jones PD, Briffa KR, Osborn TJ, Moberg A, Bergstrom H. 2002. Relationships between circulation strength and the variability of growing season and cold season climate in Northern and Central Europe. *Holocene* **12**: 657–665.

Joyce RJ, Janowiak JE, Arkin PA, Xie P. 2004. CMORPH: a method that produces global precipitation estimates from passive microwave and infrared data at high spatial and temporal resolutions. *Journal of Hydrometeorology* **5**: 487–503.

Joyce RJ, Xie P, Janowiak J. 2009. A Kalman filter approach to blend various satellite rainfall estimates in CMORPH. *Proceedings of the 4th IPWG Workshop*, 13–17 October 2009, Beijing; 178. http://www.isac.cnr.it/~ipwg/meetings/beijing/4th-IPWG-Proceedings-web-March-2009.pdf (accessed 9 August 2011).

Kahn R, Petzold A, Wendisch M, Bierwirth E, Dinter T, Esselborn M, Fiebig M, Heese B, Knippertz P, Muller D, Schladitz A, von Hoyningen-Huene W. 2008. Desert dust aerosol air mass mapping in the western Sahara, using particle properties derived from space-based multi-angle imaging. *Tellus* **61**: 239–251.

Katsumata M, Uyeda H, Iwanami K, Liu G. 2000. The response of 36- and 89-GHz microwave channels to convective snow clouds over ocean: observation and modeling. *Journal of Applied Meteorology* **39**: 2322–2335.

Kawanishi T, Sezai T, Ito Y, Imaoka K, Takeshima T, Ishido Y, Shibata A, Miura M, Inahata H, Spencer RW. 2003. The advanced microwave scanning radiometer for the earth observing system (AMSR-E), NASDA's contribution to the EOS for global energy and water cycle studies. *IEEE Transactions on Geoscience and Remote Sensing* **41**: 184–194.

Kidd C. 1998. Passive microwave rainfall monitoring using polarization-corrected temperatures. *International Journal of Remote Sensing* **19**: 981–996.

Kidd C, Bauer P, Turk J, Huffman GJ, Joyce R, Hsu K-L, Braithwaite D. Intercomparison of high resolution precipitation products over northwest Europe. *Journal of Hydrometeorology* (in press).

Kidd C, Ferraro RR, Levizzani V. 2010. The International Precipitation Working Group. *Bulletin of the American Meteorological Society* **8**: 1095–1099, DOI: 10.1175/2009BAMS2871.1.

Kidd C, Kniveton D, Barrett EC. 1998. The advantages and disadvantages of statistically derived – empirically calibrated passive microwave algorithms for rainfall estimation. *Journal of the Atmospheric Sciences* **55**: 1576–1582.

Kidd C, Kniveton DR, Todd MC, Bellerby TJ. 2003. Satellite rainfall estimation using a combined passive microwave and infrared algorithm. *Journal of Hydrometeorology* **4**: 1088–1104.

Kidd C, Levizzani V, Turk J, Ferraro R. 2009. Satellite precipitation measurements for water resource monitoring. *Journal of the American Water Resources Association* **45**: 567–579.

Kidd C, Muller C. 2009. The University of Birmingham passive microwave – infrared combined algorithm. In *Satellite Applications for Surface Hydrology*, Houssain F, Gebremichael M (eds). Springer-Verlag: Dortrecht, the Netherlands; 327.

Kidwell KB. 1991. *NOAA polar orbiter data (TIROS-N, NOAA-6, NOAA-7, NOAA-8, NOAA-9, NOAA-10, NOAA-11 and NOAA-12) User's Guide*. NOAA/NESDIS: Washington, DC. http://www.ncdc.noaa.gov/oa/pod-guide/ncdc/docs/podug/index.htm (accessed 11 May 2011).

Kitchen M, Jackson PM. 1993. Weather radar performance at long range – simulated and observed. *Journal of Applied Meteorology* **32**: 975–985.

Klaes KD, Cohen M, Buhler Y, Schlussel P, Munro R, Luntama J-P, von Engeln A, O'Clerigh E, Bonekamp H, Ackermann J, Schmetz J. 2007. An introduction to the EUMETSAT polar system. *Bulletin of the American Meteorological Society* **88**: 1085–1096.

Kniveton DR, Motta BC, Goodman HM, Smith M, LaFontaine FJ. 1994. The First WetNet Precipitation Intercomparison Project: generation of results. *Remote Sensing Reviews* **11**: 243–302.

Kongoli C, Ferraro RR, Pellegrino P, Meng H, Dean C. 2007. Utilization of the AMSU high frequency measurements for improved coastal rain retrievals. *Geophysical Research Letters* **34**: L17809, DOI: 10.1029/2007GL029940.

Krajewski WF, Anderson MC, Eichinger WE, Entekhabi D, Hornbuckle BK, Houser PR, Katul GG, Kustas WP, Norman JM, Peters-Lidard C, Wood EF. 2006. A remote sensing observatory for hydrologic sciences: a genesis for scaling to continental hydrology. *Water Resources Research* **42**: W07301.

Krajewski WF, Ciach GJ, McCollum JR, Bacotiu C. 2000. Initial validation of the Global Precipitation Climatology Project monthly rainfall over the United States. *Journal of Applied Meteorology* **39**: 1071–1086.

Kubota T, Shige S, Hashizume H, Aonashi K, Takahashi N, Seto S, Hirose M, Takayabu YN, Nakagawa K, Iwanami K, Ushio T, Kachi M, Okamoto K. 2007. Global precipitation map using satelliteborne microwave radiometers by the GSMaP Project: production and validation. *IEEE Transactions on Geoscience and Remote Sensing* **45**: 2259–2275.

Kühnlein M, Thies B, Nauß T, Bendix J. 2010. Rainfall-rate assignment using MSG SEVIRI data – a promising approach to spaceborne rainfall-rate retrieval for midlatitudes. *Journal of Applied Meteorology and Climatology* **49**: 1477–1495.

Kuligowski RJ. 2002. A self-calibrating GOES rainfall algorithm for short term rainfall estimates. *Journal of Hydrometeorology* **3**: 112–130.

Kummerow C, Barnes W, Kozu T, Shiue J, Simpson J. 1998. The Tropical Rainfall Measuring Mission (TRMM) sensor package. *Journal of Atmospheric and Oceanic Technology* **15**: 809–817.

Kummerow CD, Hong Y, Olson WS, Yang S, Adler RF, McCollum J, Ferraro R, Petty G, Shin D-B, Wilheit TT. 2001. The evolution of the Goddard Profiling Algorithm (GPROF) for rainfall estimation from passive microwave sensors. *Journal of Applied Meteorology* **40**: 1801–1820.

Kummerow C, Olson WS, Giglio L. 1996. A simplified scheme for obtaining precipitation and vertical hydrometeor profiles from microwave sounders. *IEEE Transactions on Geoscience and Remote Sensing* **34**: 1213–1232.

Kunkee DB, Poe GA, Boucher DJ, Swadley SD, Hong Y, Wessel JE, Uliana EA. 2008. Design and evaluation of the first special sensor microwave imager/sounder. *IEEE Transactions on Geoscience and Remote Sensing* **46**: 863–883.

Lambrigtsen B, Tanner A, Gaier T, Kangaslahti P, Brown S. 2007. Prototyping GeoSTAR for the PATH mission. *NASA Science Technology Conference*, 19–21 June, Adelphi, MD. http://esto.nasa.gov/conferences/nstc2007/papers/Lambrigtsen_Bjorn_B1P4_NSTC-07-0020.pdf (accessed 9 August 2011).

Laviola S, Levizzani V. 2009. Observing precipitation by means of water vapor absorption lines; A first check of the retrieval capabilities of the 183-WSL rain retrieval method. *Italian Journal of Remote Sensing* **41**: 39–49.

Laviola S, Levizzani V. 2011. The 183-WSL fast rain rate retrieval algorithm. Part I: retrieval design. *Atmospheric Research* **99**: 443–461, DOI: 10.1016/j.atmosres.2010.1011.1013.

Legates DR, Willmott CJ. 1990. Mean seasonal and spatial variability in gauge-corrected, global precipitation. *International Journal of Climatology* **10**: 111–127.

Lensky IM, Rosenfeld D. 2003a. A night-rain delineation algorithm for infrared satellite data based on microphysical considerations. *Journal of Applied Meteorology* **42**: 1218–1226.

Lensky IM, Rosenfeld D. 2003b. Satellite-based insights into precipitation formation processes in continental and maritime convective clouds at nighttime. *Journal of Applied Meteorology* **42**: 1227–1233.

Lensky IM, Rosenfeld D. 2008. Clouds-Aerosols-Precipitation Satellite Analysis Tool (CAPSAT). *Atmospheric Chemistry and Physics Discussions* **8**: 4765–4809.

Lethbridge M. 1967. Precipitation probability and satellite radiation data. *Monthly Weather Review* **95**: 487–490.

Levizzani V, Laviola S, Cattani E. 2011. Detection and measurement of snowfall from Space. *Remote Sensing* **3**: 145–166.

Levizzani V, Schmetz J, Lutz HJ, Kerkmann J, Alberoni PP, Cervino M. 2001. Precipitation estimations from geostationary orbit and prospects METEOSAT Second Generation. *Meteorological Applications* **8**: 23–41.

Liu G. 2008. Deriving snow cloud characteristics from CloudSat observations. *Journal of Geophysical Research* **113**: D00A09, DOI: 10.1029/2007JD009766.

Liu G, Curry JA. 1997. Precipitation characteristics in Greenland-Iceland-Norwegian Seas determined by using satellite microwave data. *Journal of Geophysical Research* **102**: 13987–13997.

Lovejoy S, Austin GL. 1979. The delineation of rain areas from visible and IR satellite data for GATE and mid-latitudes. *Atmosphere-Ocean* **17**: 77–92.

McCollum JR, Ferraro RR. 2005. Microwave rainfall estimation over coasts. *Journal of Atmospheric and Oceanic Technology* **22**: 497–512.

McCollum JR, Krajewski WF, Ferraro RR, Ba MB. 2002. Evaluation of biases of satellite rainfall estimation algorithms over the continental United States. *Journal of Applied Meteorology* **41**: 1065–1080.

McPhee J, Margulis SA. 2005. Validation and error characterization of the GPCP-1DD precipitation product over the contiguous United States. *Journal of Hydrometeorology* **6**: 441–459.

Mace GG, Zhang Q, Vaughan M, Marchand R, Stephens GL, Trepte C, Winker D. 2009. A description of hydrometeor layer occurrence statistics derived from the first year of merged Cloudsat and CALIPSO data. *Journal of Geophysical Research* **114**: D00A26, DOI: 10.1029/2007JD009755.

Marchand R, Mace GG, Ackerman T, Stephens GL. 2008. Hydrometeor detection using Cloudsat – an earth-orbiting 94-GHz cloud radar. *Journal of Atmospheric and Oceanic Technology* **25**: 519–533.

Marks DA, Wolff DB, Silberstein DS, Tokay A, Pippitt JL, Wang J. 2009. Availability of high-quality TRMM ground validation data from Kwajalein, RMI: a practical application of the relative calibration adjustment technique. *Journal of Atmospheric and Oceanic Technology* **26**: 413–429.

Marzano FS, Cimini D, Memmo A, Montopoli RT, Sanctis MD, Lucente M, Mortari D, Michele SD. 2009. Flower constellation of millimeter-wave radiometers for tropospheric monitoring at pseudogeostationary scale. *IEEE Transactions on Geoscience Remote Sensing* **47**: 3107–3122.

Marzano FS, Cimini D, Rossi T, Mortari D, Di Michele S, Bauer P. 2010. High-repetition millimeter-wave passive remote sensing of humidity and hydrometeor profiles from elliptical orbit constellations. *Journal of Applied Meteorology and Climatology* **49**: 1454–1476, DOI: 10.1175/2010JAMC2329.1.

Marzano FS, Palmacci M, Cimini D, Giuliani G, Turk FJ. 2004. Multivariate statistical integration of satellite infrared and microwave radiometric measurements for rainfall retrieval at the geostationary scales. *IEEE Transactions on Geoscience Remote Sensing* **42**: 1018–1032.

Masunaga H, Kummerow CD. 2005. Combined radar and radiometer analysis of precipitation profiles for a parametric retrieval algorithm. *Journal of Atmospheric and Oceanic Technology* **22**: 909–29.

Menzel WP, Purdom JFW. 1994. Introducing GOES-I: the first of a new generation of geostationary operational environmental satellites. *Bulletin of the American Meteorological Society* **75**: 757–781.

Michaelides S, Levizzani V, Anagnostou E, Bauer P, Kasparis T, Lane JE. 2009. Precipitation: measurement remote sensing, climatology and modelling. *Atmospheric Research* **94**: 512–533.

Miller SW, Arkin PA, Joyce RJ. 2001. A combined microwave/infrared rain rate algorithm. *International Journal of Remote Sensing* **22**: 3285–3307.

Mitrescu C, L'Ecuyer T, Haynes J, Miller S, Turk J. 2010. CloudSat precipitation profiling algorithm – model description. *Journal of*

Applied Meteorology and Climatology **49**: 991–1003, DOI: 10.1175/2009JAMC2181.1.

Mugnai A, Smith EA, Tripoli GJ. 1993. Foundations for statistical-physical precipitation retrieval from passive microwave satellite measurements. Part II: emission-source and generalized weighting-function properties of a time-dependent cloud-radiation model. *Journal of Applied Meteorology* **32**: 17–39.

Murao H, Nishikawa I, Kitamura S, Yamada M, Xie P. 1993. A hybrid neural network system for the rainfall estimation using satellite imagery. In *Proceedings of the International Joint Conference on Neural Networks, Nagoya, Japan*, 25–29 October 1993. IEEE Press: 1211–1212.

Nakamura K, Iguchi T. 2007. Dual-wavelength radar algorithm. In *Measuring Precipitation from Space – EURAINSAT and the Future*, Levizzani V, Bauer P, Turk FJ (eds). Springer: Dortrecht, the Netherlands; 225–234.

Nakamura K, Iguchi T, Kojima M, Smith EA. 2005. Global Precipitation Mission (GPM) and Dual-Wavelength Radar (DPR). *Proceedings of the URSI General Assembly*, New Dehli, 23–29 October. http://www.ursi.org/Proceedings/ProcGA05/pdf/F10.1(0803).pdf (accessed 9 August 2011).

Nesbitt SW, Anders AM. 2009. Very high resolution precipitation climatologies from the Tropical Rainfall Measuring Mission precipitation radar. *Geophysical Research Letters* **36**: L15815.

Nesbitt SW, Zipser EJ. 2003. The diurnal cycle of rainfall and convective intensity according to three years of TRMM measurements. *Journal of Climate* **16**: 1456–1475.

Nesbitt SW, Zipser EJ, Kummerow CD. 2004. An examination of Version-5 rainfall estimates from the TRMM Microwave Imager, Precipitation Radar, and rain gauges on global, regional, and storm scales. *Journal of Applied Meteorology* **43**: 1016–1036.

New M. 1999. Uncertainties in observed climate. In *Representing Uncertainty in Climate Change Scenarios and Impact Studies*, Carter T, Hulme M, Viner D (eds). Climatic Research Unit: Norwich; 59–66.

New M, Todd M, Hulme M, Jones P. 2001. Precipitation measurements and trends in the twentieth century. *International Journal of Climatology* **21**: 1899–1922.

Nicholson SE, Some B, McCollum J, Nelkin E, Klotter D, Berte Y, Diallo BM, Gaye I, Kpabeba G, Ndiaye O, Noupozounkou JN, Tanu MM, Thiam A, Toure AA, Traore AK. 2003a. Validation of TRMM and other rainfall estimates with a high-density gauge dataset for West Africa. Part I: validation of GPCC rainfall product and pre-TRMM satellite and blended products. *Journal of Applied Meteorology* **42**: 1337–1354.

Nicholson SE, Some B, McCollum J, Nelkin E, Klotter D, Berte Y, Diallo BM, Gaye I, Kpabeba G, Ndiaye O, Noupozounkou JN, Tanu MM, Thiam A, Toure AA, Traore AK. 2003b. Validation of TRMM and other rainfall estimates with a high-density gauge dataset for West Africa. Part II: validation of TRMM rainfall products. *Journal of Applied Meteorology* **42**: 1355–1368.

Olson WS, Kummerow CD, Hong Y, Tao W-K. 1999. Atmospheric latent heating distributions in the tropics derived from satellite passive microwave radiometer measurements. *Journal of Applied Meteorology* **38**: 633–664.

Peterson TC, Easterling DR, Karl TR, Groisman P, Nicholls N, Plummer N, Torok S, Auer I, Boehm R, Gullett D, Vincent L, Heino R, Tuomenvirta H, Mestre O, Szentimrey T, Salinger J, Forland EJ, Hanssen-Bauer I, Alexandersson H, Jones P, Parker D. 1998. Homogeneity adjustments of in situ atmospheric climate data: a review. *International Journal of Climatology* **18**: 1493–1517.

Purdom JFW, Dills PN. 1994. Cloud motion and height measurements from multiple satellites including cloud heights and motions in polar regions. In *Preprints, Seventh Conference on Satellite Meteorology and Oceanography, Monterey, CA*, American Meteorological Society: Boston, MA; 408–411.

Roebeling RA, Holleman I. 2009. SEVIRI rainfall retrieval and validation using weather radar observations. *Journal of Geophysical Research-Atmospheres* **144**: D21202.

Rosenfeld D, Gutman G. 1994. Retrieving microphysical properties near the tops of potential rain clouds by multispectral analysis of AVHRR data. *Atmospheric Research* **34**: 259–283.

Rosenfeld D, Lensky IM. 1998. Satellite – based insights into precipitation formation processes in continental and maritime convective clouds. *Bulletin of the American Meteorological Society* **79**: 2457–2476.

Rudolf B, Hauschild H, Rueth W, Schneider U, 1994. Terrestrial precipitation analysis: operational method and required density of point measurements. In *Global Precipitation and Climate Change*, Desbois M, Desalmand F (eds). Springer: Berlin; 173–186.

Sapiano MRP, Arkin PA. 2009. An intercomparison and validation of high-resolution satellite precipitation estimates with 3-hourly gauge data. *Journal of Hydrometeorology* **10**: 149–166.

Saunders RW, Hewison TJ, Stringer SJ, Atkinson NC. 1995. The radiometric characterization of AMSU-B. *IEEE Transactions on Microwave Theory Technology* **43**: 760–771.

Savage RC, Weinman JA. 1975. Preliminary calculations of the upwelling radiance from rainclouds at 37.0 and 19.35 GHz. *Bulletin of the American Meteorological Society* **56**: 1272–1274.

Schmetz J, Pili P, Tjmekes S, Just D, Kerkmann J, Rota S, Ratier A. 2002. An introduction to Meteosat Second Generation (MSG). *Bulletin of the American Meteorological Society* **83**: 977–992.

Schmit TJ, Li J, Ackerman SA, Gurka JJ. 2005. High-spectral- and high-temporal-resolution infrared measurements from geostationary orbit. *Journal Atmospheric and Oceanic Technology* **26**: 2273–2292.

Schneider U, Becker A, Meyer-Christoffer A, Ziese M, Rudolf B. 2010. *Global Precipitation Analysis of the GPCC*. Deutcher Wetterdienst: Offenbach am Main. http://www.dwd.de/bvbw/generator/DWDWWW/Content/Oeffentlichkeit/KU/KU4/KU42/en/Reports__Publications/GPCC__intro__products__2008,templateId=raw,property=publicationFile.pdf/GPCC_intro_products_2008.pdf (accessed 9 August 2011).

Smith EA, Lamm JE, Adler R, Alishouse J, Aonashi K, Barrett E, Bauer P, Berg W, Chang A, Ferraro R, Ferriday J, Goodman S, Grody N, Kidd C, Kniveton D, Kummerow C, Liu G, Marzano F, Mugnai A, Olson W, Petty G, Shibata A, Spencer R, Wentz F, Wilheit T, Zipser E. 1998. Results of WetNet PIP-2 project. *Journal of the Atmospheric Sciences* **55**: 1483–1536.

Smith EA, Mugnai A, Cooper HJ, Tripoli GJ, Xiang X. 1992. Foundations for statistical-physical precipitation retrieval from passive microwave satellite measurements. Part I: brightness-temperature properties of a time-dependent cloud-radiation model. *Journal of Applied Meteorology* **31**: 506–531.

Sohn BJ, Han H-J, Seo E-K. 2010. Validation of satellite-based high-resolution rainfall products over the korean peninsula using data from a dense rain gauge network. *Journal of Applied Meteorology and Climatology* **49**: 701–714, DOI: 10.1175/2009JAMC2266.1.

Sorooshian S, Hsu K-L, Gao X, Gupta HV, Imam B, Braithwaite D. 2000. Evaluation of PERSIANN system satellite-based estimates of tropical rainfall. *Bulletin of the American Meteorological Society* **81**: 2035–2046.

Spencer RW, Goodman HM, Hood RE. 1989. Precipitation retrieval over land and ocean with the SSM/I: identification and characteristics of the scattering signal. *Journal of Atmospheric and Oceanic Technology* **6**: 254–273.

Staelin DH, Chen FW. 2000. Precipitation observations near 54 and 183 GHz using the NOAA-15 satellite. *IEEE Transactions on Geoscience and Remote Sensing* **38**: 2322–2332.

Stephens GL, Vane DG, Boain RJ, Mace GG, Sassen K, Wang Z, Illingworth AJ, O'Connor EJ, Rossow WB, Durden SL, Miller SD, Austin RT, Benedetti A, Mitrescu C, Team TCS. 2002. The CloudSat mission and the A-Train – a new dimension of space-based observations of clouds and precipitation. *Bulletin of the American Meteorological Society* **83**: 1771–1790.

Stephens GL, Vane DG, Tanello S, Im E, Durden S, Rokey M, Reinke D, Partain P, Mace GG, Austin R, L'Ecuyer TS, Haynes J, Lebsock M, Suzuki K, Waliser D, Wu D, Kay J, Gettleman A, Wang Z, Marchand R. 2008. CloudSat mission: performance and early science after the first year of operation. *Journal of Geophysical Research* **113**: D00A18, DOI: 10.1029/2008JD009982.

Strangeways I. 2007. *Precipitation: Theory, Measurement and Distribution*. Cambridge University Press: Cambridge; 290.

Stubenrauch CJ, Eddounia F, Edwards JM, Macke A. 2007. Evaluation of cirrus parameterizations for radiative flux computations in climate models using TOVS-ScaRaB satellite observations. *Journal of Climate* **20**: 4459–4475, DOI: 10.1175/JCLI4251.1.

Stuhlmann R, Rodriguez A, Tjemkes S, Grandell J, Arriaga A, Bezy J-L, Aminou D, Bensi P. 2005. Plans for EUMETSAT's Third Generation Meteosat geostationary satellite programme. *Advances in Space Research* **36**: 975–981.

Surussavadee C, Staelin DH. 2007. Millimeter-wave precipitation retrievals and observed-versus-simulated radiance distributions: sensitivity and assumptions. *Journal of the Atmospheric Sciences* **64**: 3808–3826.

Surussavadee C, Staelin DH. 2008a. Global millimeter-wave precipitation retrievals trained with a cloud-resolving numerical weather

prediction model, part I: retrieval design. *IEEE Transactions on Geoscience and Remote Sensing* **46**: 99–108.

Surussavadee C, Staelin DH. 2008b. Global millimeter-wave precipitation retrievals trained with a cloud-resolving numerical weather prediction model, part II: performance evaluation. *IEEE Transactions on Geoscience and Remote Sensing* **46**: 109–118.

Surussavadee C, Staelin DH. 2010. Global precipitation retrievals using the NOAA AMSU millimeter-wave channels: comparisons with rain gauges. *Journal of Applied Meteorology and Climatology* **49**: 124–135, DOI: 10.1175/2009JAMC2262.1.

Susskind J, Piraino P, Rokke L, Iredell T, Mehta A. 1997. Characteristics of the TOVS Pathfinder Path A dataset. *Bulletin of the American Meteorological Society* **78**: 1449–1472.

Tapiador FJ, Kidd C, Levizanni V, Marzano FS. 2004. A neural networks-based fusion technique to estimate half-hourly rainfall estimates at 0.1° degree resolution from satellite passive microwave and infrared data. *Journal of Applied Meteorology* **43**: 576–594.

Thies B, Nauss T, Bendix J. 2008. Precipitation process and rainfall intensity differentiation using meteosat second generation spinning enhanced visible and infrared imager data. *Journal of Geophysical Research* **113**: D23206, DOI: 23210.21029/22008JD010464.

Thornes J, Bloss W, Bouzarovski S, Cai X, Chapman L, Clark J, Dessai S, Du S, van der Horst D, Kendall M, Kidd C, Randalls S. 2010. Communicating the value of atmospheric services. *Meteorological Applications* **17**: 243–250, DOI: 10.1002/met.200.

Todd MC, Barrett EC, Beaumont MJ, Bellerby TJ. 1999. Estimation of daily rainfall over the upper Nile river basin using a continuously calibrated satellite infrared technique. *Meteorological Applications* **6**: 201–210.

Todd MC, Barrett EC, Beaumont MJ, Green JL. 1995. Satellite identification of rain days over the upper Nile river basin using an optimum infrared rain no-rain threshold temperature model. *Journal of Applied Meteorology* **34**: 2600–2611.

Todd MC, Kidd C, Kniveton D, Bellerby TJ. 2001. A combined satellite infrared and passive microwave technique for estimation of small-scale rainfall. *Journal of Atmospheric and Oceanic Technology* **18**: 742–755.

Todd M, Washington R. 1999. A simple method to retrieve 3-hourly estimates of global tropical and subtropical precipitation from international satellite cloud climatology program (ISCCP) D1 data. *Journal of Atmospheric and Oceanic Technology* **16**: 146–155.

Trenberth KE, Fasullo JT, Kiehl J. 2009. Earth's global energy budget. *Bulletin of the American Meteorological Society* **90**: 311–324.

Trenberth KE, Smith L, Qian T, Dai A, Fasullo J. 2007. Estimates of the global water budget and its annual cycle using observational and model data. *Journal of Hydrometeorology* **8**: 758–769.

Turk FJ, Arkin P, Ebert EE, Sapiano M. 2008. Evaluating high-resolution precipitation products. *Bulletin of the American Meteorological Society* **89**: 1911–1916.

Turk J, Bauer P. 2006. The International Precipitation Working Group and its role in the improvement of quantitative precipitation measurements. *Bulletin of the American Meteorological Society* **87**: 643–647.

Turk FJ, Hawkins J, Smith EA, Marzano FS, Mugnai A, Levizzani V. 2000. Combining SSM/I, TRMM and infrared geostationary satellite data in a near-real time fashion for rapid precipitation updates: advantages and limitations. In *Proceedings of the 2000 EUMETSAT Meteorological Satellite Data Users' Conference, Bologna, Italy*, Vol.2. EUMETSAT: Noordwijk; 705–707.

Turk FJ, Sohn B-J, Oh H-J, Ebert EE, Levizzani V, Smith EA. 2009. Validating a rapid-update satellite precipitation analysis across telescoping space and time scales. *Meteorology Atmospheric Physics* **105**: 99–108.

Ushio T, Okamoto K. 2009. GSMAP_MVK(+)', IPWG Algorithm Inventory, 4. http://www.isac.cnr.it/~ipwg/algorithms/inventory/GSMaP.pdf (accessed 9 August 2011).

Ushio T, Sasashige K, Kubota T, Shige S, Okamoto K, Aonashi K, Inoue T, Takahashi N, Iguchi T, Kachi M, Oki R, Morimoto T, Kawasaki Z-I. 2009. A Kalman filter approach to the Global Satellite Mapping of Precipitation (GSMaP) from combined passive microwave and infrared radiometric data. *Journal of the Meteorological Society of Japan* **87A**: 137–151.

Vicente G, Davenport JC, Scofield RA. 2002. The role of orographic and parallax corrections on real time high resolution satellite rainfall rate distribution. *International Journal of Remote Sensing* **23**: 221–230.

Vicente GA, Scofield RA, Menzel WP. 1998. The operational GOES infrared rainfall estimation technique. *Bulletin of the American Meteorological Society* **79**: 1883–1898.

Wang S-Y, Chen T-C. 2008. Measuring East Asian summer monsoon rainfall contributions by different weather systems over Taiwan. *Journal Applied Meteorological Climatology* **47**: 2068–2080.

Wang JR, Racette PE, Triesky ME. 2001. Retrieval of precipitable water vapor by the millimeter-wave imaging radiometer in the Arctic region during FIRE-ACE. *IEEE Geoscience and Remote Sensing Letters* **39**: 595–605.

Wang JR, Wilheit TT. 1989. Retrieval of total precipitable water using radiometric measurements near 92 and 183 GHz. *Journal of Applied Meteorology* **28**: 146–154.

Weinman JA, Guetter PJ. 1977. Determination of rainfall distributions from microwave radiation measured by the Nimbus 6 EMSR. *Journal of Applied Meteorology* **16**: 437–442.

Weng F, Grody NC. 2000. Retrieval of ice cloud parameters using a microwave imaging radiometer. *Journal of Atmospheric Science* **57**: 1069–1081.

Weng F, Zhao L, Ferraro RR, Poe G, Li X, Grody NC. 2003. Advanced microwave sounding unit cloud and precipitation algorithms. *Radio Science* **38**: 8068, DOI: 10.1029/2002RS002679.

Wilheit TT, Chang ATC, Rao MSV, Rodgers EB, Theon JS. 1977. A satellite technique for quantitatively mapping rainfall rates over the oceans. *Journal of Applied Meteorology* **16**: 551–560.

Winker DM, Hunt WH, McGill MJ. 2007. Initial performance assessment of CALIOP. *Geophysical Research Letters* **34**: L19803, DOI: 10.1029/2007GL030135.

WMO. 2005. *World Weather Watch – Twenty-second Status Report on Implementation*. WMO: Geneva; 60, ISBN 92-63-10986-9.

Wolff DB, Marks DA, Amitai E, Silberstein DS, Fisher BL, Tokay A, Wang J, Pippitt JL. 2005. Ground validation for the Tropical Rainfall Measuring Mission (TRMM). *Journal of Atmospheric and Oceanic Technology* **22**: 365–380.

Wu MLC. 1991. Global precipitation estimates from satellite-using difference fields of outgoing long-wave-radiation. *Atmosphere-Ocean* **29**: 150–174.

Xie P, Arkin PA. 1997. Global precipitation: a 17-year monthly analysis based on gauge observations, satellite estimates, and numerical model outputs. *Bulletin of the American Meteorological Society* **78**: 2539–2578.

Xie P, Arkin PA. 1998. Global monthly precipitation estimates from satellite-observed outgoing long wave radiation. *Journal of Climate* **11**: 137–164.

Xie P, Janowiak JE, Arkin PA, Adler R, Gruber A, Ferraro R, Huffman GJ, Curtis S. 2003. GPCP pentad precipitation analyses: an experimental data set based on gauge observations and satellite estimates. *Journal of Climate* **16**: 2197–2214.

Xie PP, Rudolf B, Schneider U, Arkin PA. 1996. Gauge-based monthly analysis of global land precipitation from 1971 to 1994. *Journal of Geophysics Research, Atmosphere* **101**: 19023–19034.

Yang S, Smith EA. 2006. Mechanisms for diurnal variability of global tropical rainfall observed from TRMM. *Journal of Climate* **19**: 5190–5226.

Yin ZY, Liu XD, Zhang XQ, Chung CF. 2004. Using a geographic information system to improve Special Sensor Microwave Imager precipitation estimates over the Tibetan Plateau. *Journal of Geophysical Research, Atmospheres* **109**: D03110.

Yoshiro K. 2002. Meteorological mission of MTSAT. *Institute of Electronics, Information and Communication Engineers Technical Report* **102**: 55–58.

Zhao L, Weng F. 2002. Retrieval of ice cloud parameters using the Advanced Microwave Sounding Unit. *Journal of Applied Meteorology* **41**: 384–395.

